Available online at www.sciencedirect.com
ScienceDirect
Geochimica et Cosmochimica Acta 70 (2006) 4663–4679
Geochimica
www.elsevier.com/locate/gca

# Geochemistry of black shales from the Neoarchaean Sandur Superterrane, India: First cycle volcanogenic sedimentary rocks in an intraoceanic arc–trench complex

C. Manikyamba [a,*], R. Kerrich [b]

[a] National Geophysical Research Institute, Uppal Road, Hyderabad 500 007, India
[b] Department of Geological Sciences, University of Saskatchewan, Saskatoon, Sask., Canada S7N 5E2

Received 11 April 2006; accepted in revised form 10 July 2006

**Abstract**

The ~2.7 Ga Sandur Superterrane (SST), of the western Dharwar craton, is a collage of greenstone terranes having distinct lithotectonic associations; volcanic associations are prevalent. Fine-grained metasedimentary rocks, which are optimal for provenance studies, are sparse in greenstone terranes of this craton. However, extensive shale sequences are present in the eastern volcanic terrane (EVT) and the eastern felsic volcanic terrane (EFVT) of the SST. Within the EVT, the black shales are stratigraphically associated with black cherts, metabasalt and banded iron formation (BIF), and underlain by greywackes. Shales have compositions of tholeiitic basalt in terms of $TiO_2$, Cr, Co, Ni, V, and Sc contents, and plot near the arc basalt endmember on the Th/Sc versus Sc mixing hyperbola. In contrast, Archean average upper continental crust of Taylor and McLennan [Taylor, S.R., McLennan, S.M., 1985. *The Continental crust: Its Composition and Evolution*. Blackwell, Oxford, 307p.; Taylor, S.R., McLennan, S.M., 1995. The geochemical evolution of the continental crust. *Rev. Geophys.* **33**, 241–265], plots mid-hyperbola indicative of bimodal arc magma provenance. Accordingly, the Sandur shales likely had a catchment in an oceanic arc or back-arc dominated by tholeiitic basalts. Specifically, Nb/Th ratios 1.5–2.5 in shales are close to those of Archean arc basalts (1–4), so a plateau or ocean island basalt source, where Nb/Th >8, can be ruled out. Compositionally, cherts are shale highly diluted by silica, with positive Eu anomalies, and are interpreted to be hydrothermal sediments precipitated from reduced fluids during periods of limited siliciclastic input. In the shales, variable $SiO_2$ and $Fe_2O_3$ contents, depletions of MnO, MgO, and $Na_2O$, and positive to negative Eu anomalies, but gains of K relative to arc basalt compositions, are interpreted as due to hydrothermal alteration. Greywackes underlying the shales have two compositions. Type I is similar to the shales, whereas Type II has fractionated REE with negative Eu anomalies consistent with a cratonic granitoid catchment [Manikyamba, C., Naqvi, S.M., Moeen, S., Gnaneswar Rao, T., Balaram, V., Ramesh, S.V., Reddy, G.L.N., 1997a. Geochemical heterogeneities of metagreywackes from the Sandur schist belt: implications for active plate margin processes. *Precambrian Res.* **84**, 117–138]. Collectively, the results are in keeping with an intraoceanic arc outboard of a continental margin. During transgression the trench has a low energy shale facies with dominant arc contribution, but for regression high energy greywackes are deposited from a cratonic provenance.


## 1. Introduction and scope

Fine-grained sedimentary rocks have been used to estimate the average composition of the continental crust (CC) during Archaean and subsequent eras. A pronounced transition has been found at the Archaean-Proterozoic boundary, after which K-rich granites apparently contributed significantly to the sedimentary budget. (Taylor and McLennan, 1981, 1985; Condie et al., 1991, 2001; Rudnick and Gao, 2004 and references therein). In contrast, Gibbs et al. (1986) reported cratonic sedimentary compositions from Archaean cratons, and bimodal volcanic arc type turbidites in Proterozoic greenstone terranes. According to Condie (1993), Archaean greenstones are more

* Corresponding author. Fax: +91 40 27171564/23434651.
*E-mail address:* cmaningri@yahoo.com (C. Manikyamba).

0016-7037/$ - see front matter © 2006 Elsevier Inc. All rights reserved.
doi:10.1016/j.gca.2006.07.015

analogous to young island arcs rather than average Archaean upper crust. He suggested that greenstone successions contain more than 50% submarine basaltic and komatiitic volcanics; the majority of the basalts are similar to basalts from oceanic arcs. The prefix meta is implicit below for all lithologies.

Previous studies of siliciclastic sedimentary (greywackes) rocks from greenstone belts of the Dharwar Craton signify a mixed cratonic source consisting of tonalite, trondhjemite, granodiorite (TTG), and mafic-ultramafic rocks of older greenstone belts (Naqvi et al., 1983, 1988; Arora et al., 1994; Manikyamba et al., 1997a). Enrichment in transition metals such as Ni, Cr and Co were contributed from older mafic-ultramafic greenstone terranes dated at 3.4 Ga by Peucat et al. (1995) and Nutman et al. (1996). Further, negative Eu anomalies are found even in 3.4 Ga sedimentary rocks where no K-rich granites are exposed (Naqvi et al., 1983; Gao and Wedepohl, 1995). In contrast, there are two types of shale in the 2.7 Ga Abitibi greenstone terrane, neither with Eu anomalies: a high Mg, Cr, Ni-type interpreted as fans shed from komatiite–basalt sequences of ocean plateaus erupted from mantle plumes, and a low Mg, Cr, Ni-type regarded as trench turbidites paired to bimodal arcs (Feng and Kerrich, 1990; Feng et al., 1993). Both are internal to the belt, and the latter is compositionally similar to average Archean sedimentary rock of Taylor and McLennan (1985).

Greywackes are present in all Neoarchaean greenstone belts of the Dharwar craton, whereas well-preserved shales that are optimal for provenance and weathering studies are rare (Taylor and McLennan, 1985; Naqvi et al., 1988; Manikyamba et al., 1997a). However, exceptions are the Shimoga and Sandur greenstone belts with extensive shale sequences. Accordingly, in this paper we report comprehensive major and trace element data for shales of the Sandur belt with two objectives: (1) assess the provenance, whether cratonic, intraoceanic, or mixed, and hence evaluate the geodynamic setting, and (2) assess hydrothermal leaching or inputs to siliciclastic rocks.

## 2. Geological setting

The Archaean Dharwar craton of India has been divided into western and eastern sectors, separated by the Closepet granite (Radhakrishna and Naqvi, 1986; Naqvi and Rogers, 1987; Naqvi, 2005). The Sandur Superterrane (SST), or composite tectonostratigraphic terranes (formerly termed greenstone belt), is situated in the eastern part of the western Dharwar craton. Volcanic rocks are prevalent and metasedimentary rocks subordinate in these belts (Fig. 1). Though black shales occur as thin units in many belts, extensive well-preserved black shale sequences are present only in the Shimoga and Sandur greenstone belts.

Archaean Superterranes, or subprovinces, are composite tectonostratigraphic terranes. Each terrane has its own characteristic combination of lithologies, stratigraphic succession, and structural-metamorphic history (Table 1; Jackson and Fyon, 1991; Manikyamba and Naqvi, 1996, 1997; Subba Rao et al., 2001; Naqvi et al., 2002a). The Sandur Superterrane is 35 km wide by 10 km in strike length, and has been studied in some detail (Manikyamba and Naqvi, 1996; Naqvi et al., 2002a,b). All characteristic lithologies of Neoarchaean greenstone terranes are present. Volcanic sequences include mafic and ultramafic flows, massive and pillowed basalts, and intermediate-felsic rocks such as andesites, rhyolites, and adakites. Sedimentary rocks include arenites, turbidites, shales, stromatolitic carbonates, banded iron formation (BIF), banded manganese formation (BMF) and chert (Table 1).

For the Sandur Superterrane, eight component terranes are juxtaposed together along three accretionary structures (Manikyamba and Naqvi, 1996; Manikyamba et al., 1997a). Lithological characteristics, structural parameters, and metamorphic grade show abrupt changes across terrane boundaries. Layer parallel structures recognized by previous workers (Fig. 1, Table 1, Chadwick et al., 1996; Manikyamba and Naqvi, 1996; Mukhopadhyay and Matin, 1996), are now interpreted as accretionary structures (Naqvi et al., 2002a,b).

Zircons from felsic volcanics of the eastern felsic volcanic terrane (EFVT) have yielded an imprecise U-Pb SHRIMP age of 2.7 Ga, and high-Mg basalts and komatiites from the Sultanpura volcanic terrane (SVT) yield a poorly defined Sm/Nd isotopic isochron with a date of 2.7 Ga (Nutman et al., 1996; Naqvi et al., 2002a). The assembled supracrustal terranes have been intruded by a series of granitoid bodies. Ages of the granitoids are still not available excepting one exposed in the EFVT ($2719 \pm 40$ Ma; Nutman et al., 1996).

The Sandur Superterrane has three phases of deformation (Mukhopadhyay and Matin, 1993), and metamorphic grade varies from greenschist facies to upper amphibolite facies depending on the terrane (Manikyamba and Naqvi, 1997; Manikyamba et al., 1997a; Table 1).

## 3. Sample design

Fine-grained sedimentary rocks are optimal for provenance and weathering studies, given the potential for heavy mineral sorting in coarser facies (Taylor and McLennan, 1985). Extensive shale sequences are present only in the EVT and EFVT. In both terranes shales, with variable proportions of carbonaceous compounds, are interbedded with black chert, and ferrugeneous pyritic chert (Table 1; Kerrich et al., 2006). Weathering of sedimentary rocks, especially in hot climates with high rainfall, is of concern for disturbing primary geochemical signatures (Holland, 1978). Consequently, we collected six samples of black shales along with three black cherts from fresh outcrops in a railway line cutting at Bhimangundi (EVT: E 76°6′ 13″; N 15°7″ 27″; samples C1, C4, C5, C8, C9, C10, and C2, C3, C7), and 10 samples of black shales from fresh outcrops in a road cutting at Vibhutigudda (EFVT: E 76°43′10″; N15°10′12″; Fig. 1; C12, 13, 14, 15, 17, 18, 20,

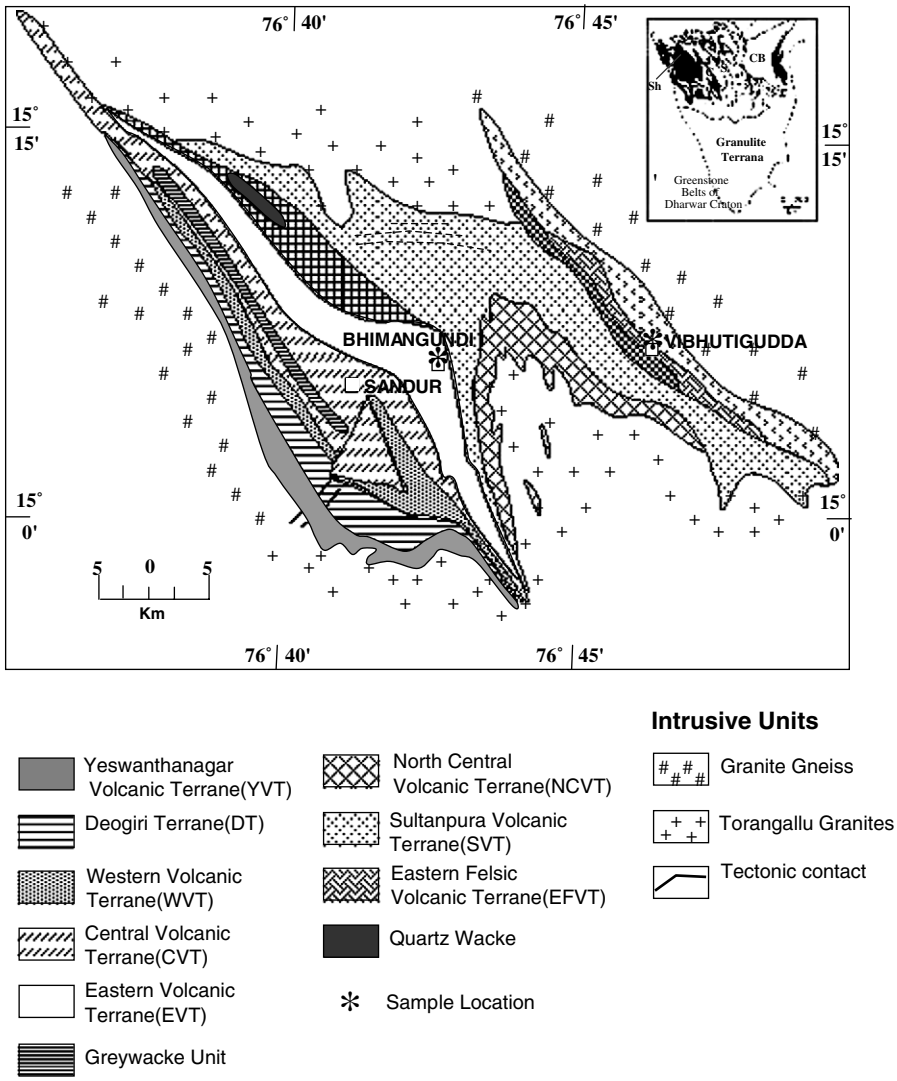


Fig. 1. Geological map of the Sandur Superterrane, showing the distribution of lithologies, and the location of two sites on either side of the SVT where unweathered samples of black shale were collected. Inset: Generalized geological map of southern Peninsular India showing the location of the Sandur Superterrane (SST); Sh, Shimoga; CB, Cuddapah basin.

21, 22, 23; Table 1; Fig. 1). These shales are fine-grained laminated metasedimentary rocks with an assemblage of quartz, tremolite, amphibole, biotite, and opaques. Preferred dimensional alignment of layer silicates defines the lamination to which S1 schistosity is parallel. Hydrothermal alteration associated with gold mineralization, generally structurally hosted, is sporadically present in many Archean greenstone terranes, including the SST (Manikyamba et al., 1997b). The two sampling locations for shales were selected to be distal from gold mineralization and structures, and the samples were devoid of veins.

## 4. Analytical methods

Major elements were determined by X-ray fluorescence spectrometry (XRF). Trace elements including the REEs and high field strength elements (HFSEs: Th, Nb, Ta, Zr, and Hf) were analysed using inductively coupled plasma mass spectrometry (ICP-MS; Perkin-Elmer ELAN 5000) at the Department of Geological Sciences, University of Saskatchewan. Detailed analytical methodology is presented in Fan and Kerrich (1997). Detection limits, defined as $3\sigma$ of the procedural blank, for some critical elements, in parts per million, are as follows: Th (0.01), Nb (0.006), Hf (0.008), Zr (0.004), La (0.01), and Ce (0.009). Precision for most elements at the concentrations present in the international reference material BCR-2 is between 2% and 6% relative standard deviation. Table 2 lists values obtained for trace elements and REE in BCR-2 and recommended values. For normalization, values for Archaean upper continental crust (AUCC) were obtained from Taylor and McLennan (1985). Chondrite normalized (e.g. $La/Sm_n$) and primitive mantle normalized ratios ($Th/Nb_{pm}$) are calculated from the values of Sun and McDonough (1989). The Chemical Index of Alteration (CIA) was calculated as $[Al_2O_3/(Al_2O_3 + CaO + Na_2O +$

Table 1
Tectonostratigraphic elements of the Sandur superterrane, with terrane bounding structures, Western Dharwar Craton

| Terrane bounding structures/Terrane | Age Ma/Ga | Major lithologies | Minor units | Volcanic/sedimentary structures | Syn-volcanic mafic intrusive | Metamorphic grade | Tectonic structures | Structural grain | Ref. |
|---|---|---|---|---|---|---|---|---|---|
| Yeswanthanagar Volcanic terrane (YVT) | ~2.7 | Amphibolites | Cr–mica quartzite | Amygdales, deformed pillows | Dunite, Peridotite | Upper amphibolite, | S1–S3 | NNW–SSE | 1 |
| Deogiri terrane (DT) | | | BMF,BIF, quartzite, greywacke, carbonate | Current bedding, ripple marks, Stromatolites | Dolerite, gabbro, pyroxenite dykes | Amphibolite-Lower greenschist | S1–F3, S1 | NW–SE | |
| Western volcanic terrane (WVT) | | Basalts, siliciclastics | BIF, shales, GIF,PIF | Graded bedding | Dolerite, gabbro, pyroxenite dykes | Lower greenschist | F1–F2, S1 | NW–SE | 2 |
| Central volcanic terrane (CVT) | | Basalts | Greywackes | Stretched pillows | Dolerite | Amphibolite | S1–F2 | NW–SE | |
| *Sandur discontinuity* | | | | | | | | | |
| Eastern volcanic terrane (EVT) | | Basalts | BIF, shales, C-shales[a] | | Dolerite | Upper greenschist | S1,F1–F2 | NW–SE | |
| *Timmappanagundi* | | | | | | | | | |
| North central Volcanic terrane (NCVT) | ~2.7 | Intermediate to felsic volcanic rocks | Fe-cherts, conglomerates, shales, greywackes, arenite- quartzwacke | Graded bedding | Dolerite | Lower greenschist | S1–F2 | ENE–WSW | |
| *Joga* | | | | | | | | | |
| Sultanpura volcanic terrane (SVT) | $2.706 \pm 184$ | Basalts, ultramafics | Cherts | Pillows | Gabbro, dolerite | Upper amphibolite | S1–F2 | E–W | |
| *Vibhutigudda* | | | | | | | | | |
| Eastern felsic volcanic terrane (EFVT) | $2.719 \pm 40$ | Basalts, felsic volcanic rocks | Conglomerates, greywacke, C-shales[b], quartzites | Variolites, graded bedding | Dolerite, pyroxenite | Garnet amphibolite | S1–F2 | NW–SE | 3 |

Banded iron formation (BIF); banded manganese formation (BMF); granular iron formation (GIF); peloidal iron formation (PIF); carbonaceous shales (C-Shales); ferrugenous chert (Fe-cherts); References: 1, Manikyamba and Naqvi (1997); 2, Naqvi et al. (2002a); 3, Nutman et al. (1996).

[a] Bhimangundi.

[b] Vibhutigudda sampling localities. F1: first generation tight isoclinal folds have steep plunges, and the regional schistosity (S1) is parallel to the axial surface of these folds. F2: second generation folds are minor and coaxial to first generation folds, where S2 schistosity is sub-parallel to S1. F3: third generation folds are km scale wavelength warps.

Table 2
Precision obtained for Trace and REE for BCR-2

| Element | A | B | SD | RSD% |
|---|---|---|---|---|
| Sc | 38.5 | 33 | 3.59 | 9.32 |
| V | 477 | 416 | 36.42 | 7.63 |
| Rb | 49.6 | 48 | 3.34 | 6.74 |
| Sr | 366 | 346 | 20.48 | 5.60 |
| Y | 35.2 | 37 | 1.67 | 4.74 |
| Zr | 193 | 188 | 11.08 | 5.73 |
| Nb | 14.05 | 10.9 | 1.12 | 7.99 |
| Cs | 1.11 | 1.1 | 0.05 | 4.72 |
| Ba | 678 | 683 | 13.33 | 1.97 |
| La | 25.22 | 25 | 0.45 | 1.79 |
| Ce | 54.66 | 53 | 1.13 | 2.07 |
| Pr | 7.06 | 6.8 | 0.22 | 3.10 |
| Nd | 29.29 | 28 | 1.08 | 3.70 |
| Sm | 6.67 | 6.7 | 0.33 | 5.00 |
| Eu | 2.00 | 2.0 | 0.07 | 3.44 |
| Gd | 7.15 | 6.8 | 0.19 | 2.64 |
| Tb | 1.04 | 1.07 | 0.03 | 2.73 |
| Dy | 6.46 | 6.0 | 0.23 | 3.61 |
| Ho | 1.31 | 1.33 | 0.06 | 4.33 |
| Er | 3.76 | 3.6 | 0.14 | 3.66 |
| Tm | 0.54 | 0.54 | 0.03 | 5.70 |
| Yb | 3.39 | 3.5 | 0.21 | 6.28 |
| Lu | 0.50 | 0.51 | 0.03 | 5.66 |
| Hf | 5.45 | 4.8 | 0.46 | 8.45 |
| Ta | 0.92 | 0.63 | 0.19 | 21.09 |
| Pb | 10.7 | 11 | 0.50 | 4.67 |
| Th | 5.98 | 6.2 | 0.24 | 3.96 |
| U | 1.65 | 1.69 | 0.05 | 3.04 |
| Cr | 66 | 18 | 25.29 | 38.15 |
| Co | 41 | 37 | 4.52 | 10.92 |
| Ni | 12.9 | 12.7 | 1.82 | 14.11 |
| Cu | 17 | 19 | 5.05 | 29.33 |
| Zn | 117 | 127 | 13.78 | 11.72 |

A, average of 14 analyses; B, reported values from Gao et al. (2002).

$K_2O)] \times 100$, corrected for diagenetic addition of K, following Fedo et al. (1995).

## 5. Results

Compositionally, there are two populations corresponding to sample descriptions of shales and cherts. The shale population I is aluminous with Ce > 14 ppm, whereas cherts are dominated by silica, having low $Al_2O_3$ and Ce < 5 ppm. Shales have relatively uniform contents of $SiO_2$, $Al_2O_3$, and $TiO_2$ systematic depletions of MgO, MnO, CaO, and $Na_2O$ relative to Archean upper continental crust (AUCC), with large variations of Fe (1.4–14.9 wt% $Fe_2O_3$). Shales are "tholeiitic basalt" in composition in terms of the contents of all of $TiO_2$, $Al_2O_3$, Th, REE, Y, Cr, Co, Ni, Sc, and V. On stacked plots ranked by ppm Ce, there are coherent trends of increasing incompatible element contents, including Th, Nb, and Zr, and of total REE; those are inherited magmatic trends (Fig. 2).

Most shales have near-flat REE patterns at 0.4–1.1 × AUCC, or mild LREE depletion; two samples show relative HREE enrichment. REE contents are not controlled by dilution from possible hydrothermal additions of Si and Fe, nor of enrichment by possible leaching of major elements. Similarly, multielement plots are coherent and near-flat, excepting variable normalized enrichments of U but troughs at Nb–Ta, and minor peaks are Zr–Hf, and Ti in some samples. The second feature may reflect winnowing of a Nb-rich heavy mineral (Fig. 3A and B; Table 3). Five samples show relatively low, or erratic HREE-enriched, patterns in conjunction with large positive anomalies at Zr, Hf, and Ti (Fig. 3C and D), and are discussed below.

Mineralogically, cherts are microcrystalline quartz, and compositionally dominated by silica (>97 wt%). Rare earth element patterns are variably concave down at 0.05–0.1 AUCC. Multielement patterns are irregular, in part due to low abundances of many elements. In view of the stratigraphic interlayering of cherts with shales, to a first approximation cherts can be viewed as a siliciclastic shale component highly diluted by hydrothermal Si during an interval of low siliciclastic input. Pronounced positive Eu anomalies signify a reducing hydrothermal fluid (Fig. 3E and F; Table 3).

## 6. Discussion

### 6.1. Provenance

Taylor and McLennan (1985, 1995) have demonstrated that for many fine-grained siliciclastic sequences the budget of REE, Th, Sc, and Co is quantitatively transferred from the provenance to the depositional basin. The covariant trends of incompatible elements in Fig. 2, and coherent plots in Fig. 3A and B indicate that these elements are appropriate for provenance studies of the Sandur shales. Sandur shales plot in the Archean field on discrimination diagrams (Fig. 4). Taylor and McLennan further showed that for many Archean greenstone belts, shale compositions plot on mixing hyperbolae between bimodal endmembers of basalt and dacite-tonalite that are prevalent lithologies in greenstone belts, as for Th/Sc vs Sc (Fig. 5).

In terms of $TiO_2$, $Al_2O_3$, REE, Cr, Co, Ni, Sc, and V contents the shales are basaltic in composition, specifically Archean low-K and medium-K series arc basalts (LKS, MKS; Hollings and Kerrich, 2006; Table 3). If this interpretation is correct, then the covariant trends in Fig. 2 arise from mixing between low Th, Nb, LREE (LKS, Ce < 20 ppm) and medium Th, Nb, LREE (MKS, Ce 21–50 ppm) endmembers which are prevalent in Archean intraoceanic arc basalt sequences (Manikyamba et al., 2004; Hollings and Kerrich, 2004, 2006), albeit with some "noise" from weathering and hydrothermal alteration on other major elements. That feature is endorsed by the average population I shale plotting near the arc basalt averages on the Th/Sc vs Sc diagram (Fig. 5).

Preservation of some primary magmatic trends is further confirmed by the correlation matrix (Table 4): (1) Zr and Nb are correlated with LREE ($r > 0.69$); (2) Th is correlat-

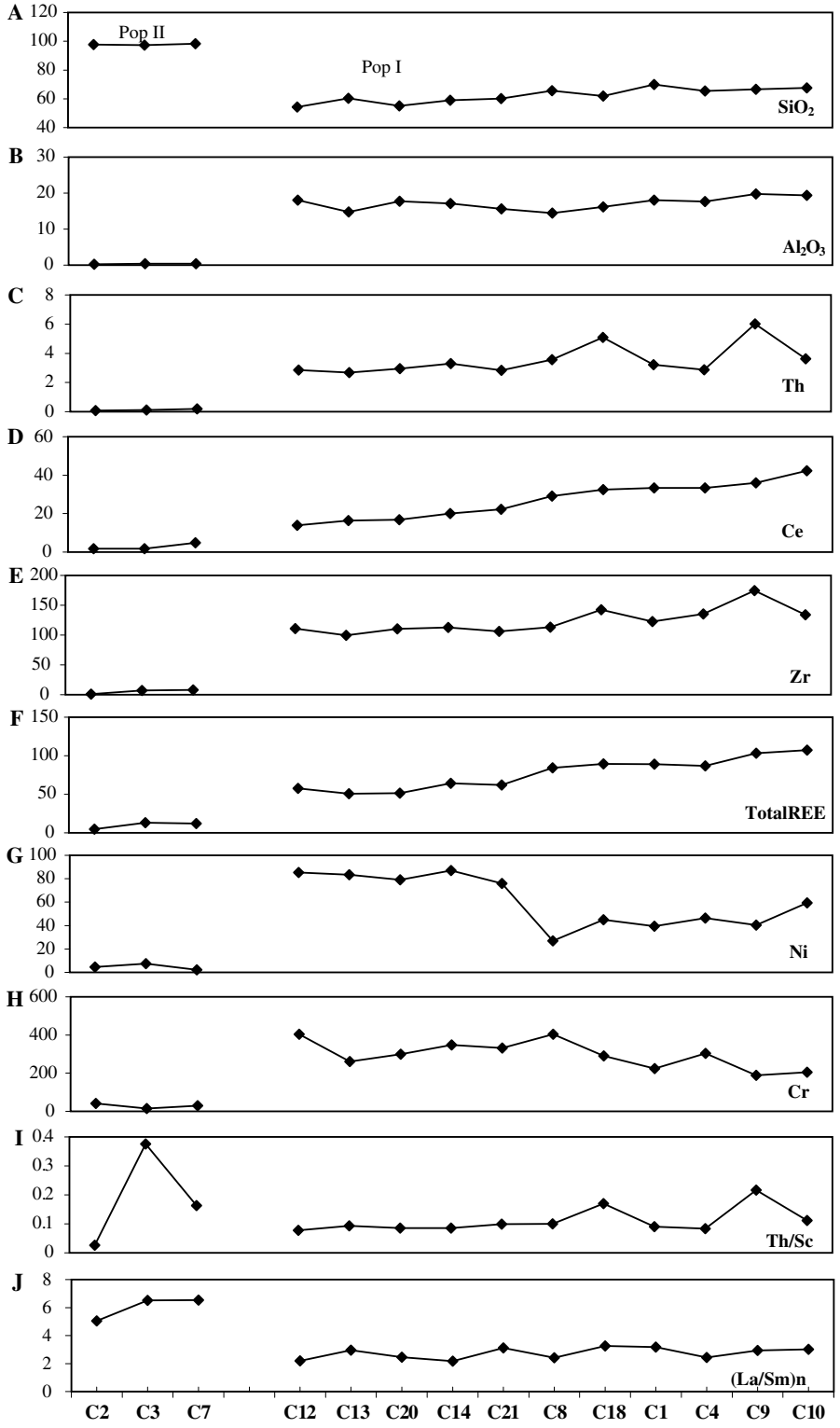


Fig. 2. Stacked diagrams, ranked by increasing Ce, of selected elements and ratios illustrating the division into population I shales and population II cherts. In population I, incompatible elements, and total REE, covary. Five samples having Zr/Sm > 60 are not plotted as discussed in the text.

ed with Nb, La, Zr, and Hf ($r > 0.78$); (3) Cr, Co, Ni, Sc, and V are correlated with $Fe_2O_3$ ($r > 0.61$) and MgO ($r > 0.51$); and (3) Cr, Co, Ni, Sc, and V are anticorrelated with $SiO_2$ ($r = -0.18$ to $-0.80$). A plateau basalt endmember can be ruled out given Nb contents of 3–8 ppm and Nb/Th ratios greater than the primitive mantle value of 8, whereas Archean arc basalts possess ratios <6, and the shales have ratios of 1.5 to 2.5. Similarly, an ocean island basalt (OIB) provenance can be eliminated from the characteristic high Nb content (average 48 ppm) and

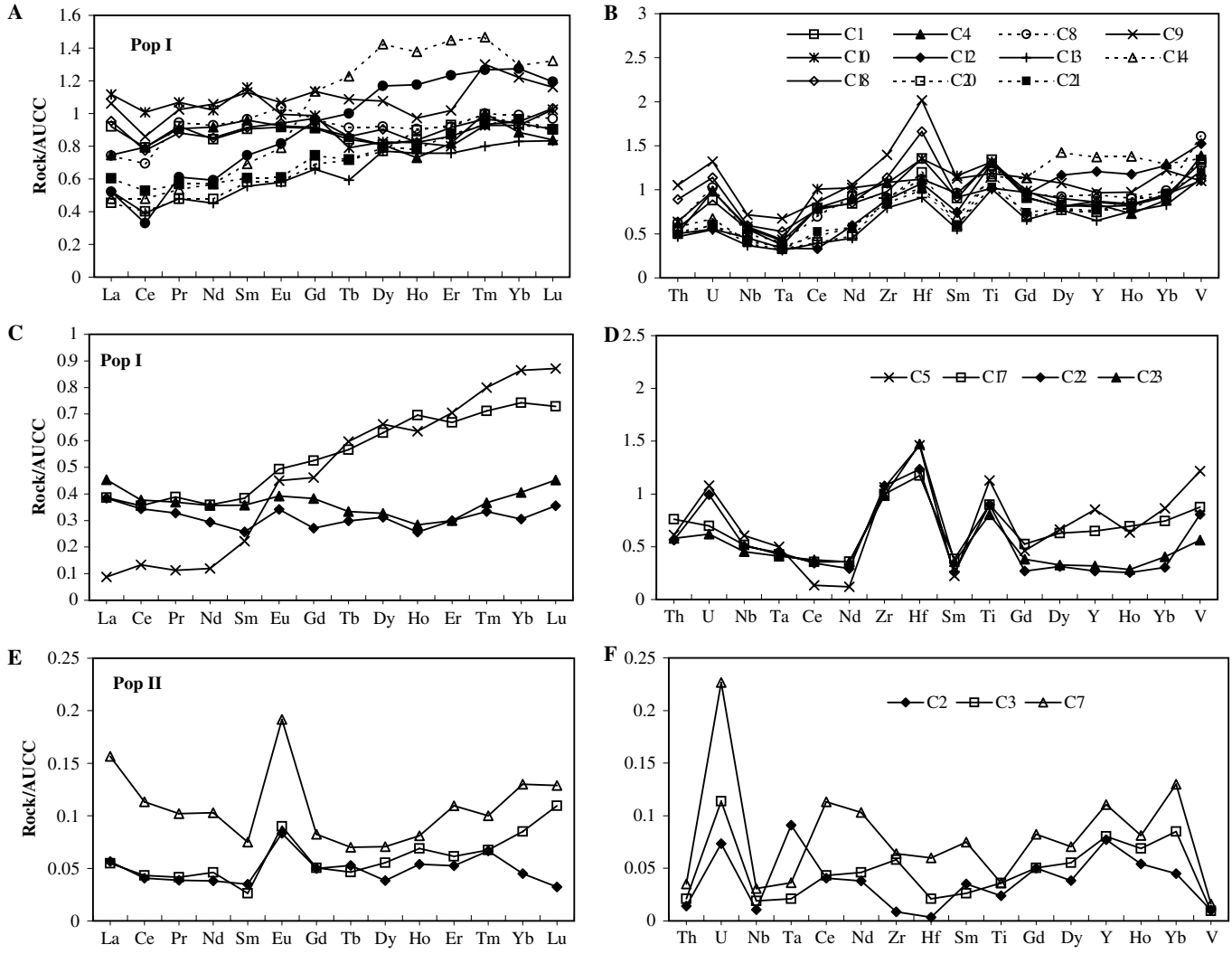


Fig. 3. AUCC normalized diagrams. A, B plots for population I shales with Zr/Sm < 60; C, D, plots for 4 of 5 samples where Zr/Sm > 60; E, F, plots for population II cherts

Nb/Th ratios (average 12) (Table 3; Sun and McDonough, 1989; Kerrich and Xie, 2002).

The most straightforward interpretation is that Sandur shales are compositionally distal trench turbidites shed off an intraoceanic arc dominated by tholeiitic LKS and MKS basalts. Alternative scenarios involving mixing between a mafic arc basalt endmember and felsic igneous debris shed off a continental shelf interpreted to have been to the east are discussed below.

### 6.2. Comparison with greywackes

Greywackes stratigraphically underlie black shales in the Vibhutigudda sampling region of the EFVT (Manikyamba et al., 1997a). These greywackes show complex compositions, and variable MgO (9.82–16.47 wt%) and $Fe_2O_3$ (3.28–21.24 wt%) contents. Negative Nb–Ta anomalies are found along with positive Zr and Hf anomalies, the former a magmatic arc signature, as against continental crust, given Cr, Co, Ni contents, and the latter zircon accumulation in high energy facies.

Manikyamba et al. (1997a) identified two compositional types of greywacke. Type I is characterized by tholeiitic basalt compositions in terms of $Al_2O_3$, $TiO_2$, Th, REE, Cr, Co, Ni, V, and Sc contents, with mildly fractionated $La/Yb_n < 3$, and devoid of Eu anomalies, whereas Type II has a lower mafic element budget, larger negative Nb anomalies, negative Eu anomalies, and $La/Yb_n = 7–16$. They interpreted Type I as forearc sediments and Type II as having a catchment dominated by felsic volcanic rocks, inferred to be a continental shelf present east of the Sandur Superterrane (Manikyamba et al., 1997a; Naqvi et al., 2002a).

The Nb content of island arc tholeiitic basalts (IAB) varies between 1–3 ppm (Pears and Peate, 1995), and similarly for inferred Archean IAB (Hollings and Kerrich, 2004; Manikyamba et al., 2004), such that an arc basalt is appropriate as an endmember for both Type I greywackes and population I shales of this study (Fig. 5). The presence of

Table 3
Chemical composition of Black Shales and Cherts from the Sandur Superterrane

| | Pop I | | | | | | | | | | | | | | | | Pop II | | |
|---|---|---|---|---|---|---|---|---|---|---|---|---|---|---|---|---|---|---|---|
| | C12(V) | C22 (V) | C17 (V) | C23 (V) | C13 (V) | C20 (V) | C14 (V) | C21 (V) | C15 (V) | C8 (B) | C18 (V) | C1 (B) | C4 (B) | C9 (B) | C10 (B) | C5 (B) | C2 (B) | C3 (B) | C7 (B) |
| $SiO_2$ | 54.27 | 70.65 | 65.41 | 73.74 | 60.28 | 54.97 | 58.90 | 60.09 | 70.80 | 65.60 | 61.85 | 69.84 | 65.43 | 66.66 | 67.58 | 69.84 | 97.75 | 97.30 | 98.25 |
| $TiO_2$ | 1.09 | 0.75 | 0.75 | 0.67 | 0.84 | 0.98 | 0.96 | 0.86 | 0.73 | 1.06 | 0.85 | 1.12 | 1.09 | 0.99 | 1.10 | 0.94 | 0.02 | 0.03 | 0.03 |
| $Al_2O_3$ | 18.07 | 17.02 | 16.62 | 16.06 | 14.78 | 17.72 | 17.10 | 15.60 | 17.58 | 14.47 | 16.19 | 18.07 | 17.63 | 19.73 | 19.39 | 13.59 | 0.24 | 0.37 | 0.39 |
| $Fe_2O_3$ | 14.86 | 1.96 | 7.51 | 1.38 | 14.67 | 14.53 | 11.81 | 13.14 | 1.41 | 11.76 | 13.52 | 2.72 | 8.53 | 4.44 | 3.65 | 9.29 | 1.15 | 1.22 | 0.40 |
| MnO | 0.10 | 0.00 | 0.02 | 0.00 | 0.09 | 0.14 | 0.09 | 0.10 | 0.10 | 0.00 | 0.01 | 0.00 | 0.00 | 0.00 | 0.10 | 0.00 | 0.00 | 0.10 | 0.10 |
| MgO | 1.70 | 0.19 | 0.58 | 0.17 | 1.71 | 1.85 | 1.32 | 1.63 | 0.19 | 0.20 | 0.19 | 0.23 | 0.19 | 0.15 | 0.16 | 0.14 | 0.07 | 0.05 | 0.05 |
| CaO | 0.81 | 0.50 | 0.37 | 0.36 | 0.26 | 0.47 | 0.35 | 0.29 | 0.51 | 0.01 | 0.60 | 0.69 | 0.64 | 0.73 | 0.70 | 1.04 | 0.02 | 0.10 | 0.00 |
| $K_2O$ | 2.13 | 2.29 | 1.86 | 1.66 | 1.19 | 1.23 | 2.58 | 1.63 | 1.80 | 1.62 | 1.68 | 2.02 | 1.96 | 2.15 | 2.09 | 0.67 | 0.04 | 0.06 | 0.08 |
| $Na_2O$ | 0.27 | 0.97 | 0.66 | 0.77 | 0.17 | 0.21 | 0.27 | 0.19 | 0.73 | 0.53 | 0.61 | 0.67 | 0.66 | 0.76 | 0.69 | 0.44 | 0.01 | 0.10 | 0.02 |
| $P_2O_5$ | 0.03 | 0.00 | 0.02 | 0.00 | 0.03 | 0.03 | 0.03 | 0.02 | 0.10 | 0.03 | 0.04 | 0.00 | 0.00 | 0.02 | 0.10 | 0.01 | 0.00 | 0.10 | 0.00 |
| LOI | 6.90 | 5.80 | 6.20 | 5.80 | 6.20 | 7.90 | 6.70 | 6.75 | 6.35 | 4.45 | 4.55 | 4.75 | 4.45 | 4.50 | 4.75 | 4.05 | 0.80 | 1.00 | 0.80 |
| Sum | 100.23 | 100.13 | 100 | 100.61 | 100.22 | 100.03 | 100.11 | 100.30 | 100.30 | 99.73 | 100.09 | 100.11 | 100.58 | 100.13 | 100.31 | 100.01 | 100.10 | 100.43 | 100.12 |
| CIA(crtd) | 81 | 77 | 82 | 81 | 88 | 88 | 82 | 86 | 81 | 85 | 81 | 80 | 80 | 80 | 81 | 80 | 71 | 47 | 77 |
| Be | n.d. | 0.50 | ud | 1.27 | ud | ud | n.d. | 0.30 | ud | 0.74 | 1.00 | 0.66 | 0.55 | 1.32 | ud | 0.84 | nd | ud | ud |
| Li | 58 | 47 | 33 | 21 | 59 | 67 | 48 | 69 | 60 | 7.49 | 28 | 30 | 32 | 33 | 33 | 47 | 0.50 | ud | 12 |
| Rb | 148 | 114 | 79 | 83 | 73 | 84 | 178 | 70 | 90 | 83 | 81 | 102 | 43 | 101 | 103 | 31 | 0.51 | 1.81 | 1.58 |
| Sr | 38 | 64 | 76 | 64 | 33 | 36 | 37 | 33 | 62 | 91 | 119 | 90 | 76 | 125 | 98 | 80 | 5.19 | 4.64 | 7.50 |
| Cs | 5.65 | 4.46 | 2.78 | 3.33 | 3.13 | 3.66 | 7.31 | 3.31 | 3.59 | 4.58 | 4.16 | 5.52 | 0.62 | 5.51 | 5.56 | 0.79 | 0.03 | 0.07 | 0.19 |
| Ba | 160 | 238 | 238 | 171 | 132 | 124 | 167 | 131 | 196 | 174 | 197 | 226 | 184 | 262 | 236 | 87 | 26 | 20 | 19 |
| Y | 22 | 5 | 12 | 6 | 12 | 13 | 25 | 14 | 8 | 17 | 15 | 16 | 15 | 17 | 15 | 15 | 1.39 | 1.45 | 1.99 |
| Zr | 111 | 135 | 125 | 123 | 99 | 110 | 113 | 106 | 128 | 113 | 143 | 123 | 136 | 174 | 134 | 133 | 1.07 | 7.29 | 7.98 |
| Hf | 3.22 | 3.70 | 3.52 | 4.42 | 2.73 | 3.59 | 3.07 | 3.00 | 3.70 | 3.36 | 4.98 | 4.07 | 3.36 | 6.05 | 4.05 | 4.38 | 0.01 | 0.06 | 0.18 |
| Nb | 5.91 | 6.55 | 6.70 | 5.88 | 4.79 | 5.92 | 5.43 | 5.13 | 6.64 | 6.46 | 7.73 | 7.21 | 7.33 | 9.32 | 7.56 | 7.89 | 0.14 | 0.25 | 0.40 |
| Ta | 0.37 | 0.49 | 0.47 | 0.45 | 0.34 | 0.36 | 0.39 | 0.35 | 0.47 | 0.45 | 0.58 | 0.41 | 0.46 | 0.74 | 0.48 | 0.55 | 0.10 | 0.02 | 0.04 |
| Th | 2.86 | 3.20 | 4.34 | 3.30 | 2.68 | 2.95 | 3.29 | 2.83 | 4.62 | 3.56 | 5.08 | 3.22 | 2.87 | 6.01 | 3.63 | 3.48 | 0.08 | 0.12 | 0.20 |
| U | 0.83 | 1.49 | 1.05 | 0.93 | 0.82 | 0.90 | 1.01 | 0.91 | 1.19 | 1.54 | 1.71 | 1.32 | 1.48 | 1.98 | 1.48 | 1.62 | 0.11 | 0.17 | 0.34 |
| La | 10.45 | 7.67 | 7.72 | 9.06 | 10.49 | 9.09 | 9.58 | 12.07 | 13.16 | 14.87 | 19.06 | 18.42 | 14.94 | 21.22 | 22.32 | 1.76 | 1.13 | 1.10 | 3.13 |
| Ce | 13.86 | 14.43 | 14.93 | 15.85 | 16.44 | 16.88 | 20.11 | 22.18 | 23.01 | 29.14 | 32.55 | 33.32 | 33.33 | 36.06 | 42.28 | 5.62 | 1.71 | 1.82 | 4.76 |
| Pr | 2.99 | 1.61 | 1.90 | 1.81 | 2.35 | 2.34 | 2.63 | 2.79 | 2.89 | 4.63 | 4.32 | 4.52 | 4.45 | 5.02 | 5.24 | 0.55 | 0.19 | 0.20 | 0.50 |
| Nd | 11.87 | 5.87 | 7.18 | 7.14 | 9.02 | 9.55 | 11.37 | 11.47 | 10.90 | 18.56 | 17.03 | 16.84 | 18.34 | 21.14 | 20.41 | 2.40 | 0.76 | 0.92 | 2.06 |
| Sm | 2.98 | 1.03 | 1.53 | 1.43 | 2.22 | 2.33 | 2.77 | 2.42 | 2.02 | 3.86 | 3.66 | 3.62 | 3.84 | 4.52 | 4.64 | 0.89 | 0.14 | 0.11 | 0.30 |
| Eu | 0.98 | 0.41 | 0.59 | 0.47 | 0.70 | 0.70 | 0.95 | 0.73 | 0.61 | 1.25 | 1.13 | 1.10 | 1.11 | 1.28 | 1.19 | 0.54 | 0.10 | 0.11 | 0.23 |
| Gd | 3.24 | 0.92 | 1.78 | 1.30 | 2.24 | 2.35 | 3.86 | 2.53 | 1.79 | 3.28 | 3.30 | 3.09 | 3.11 | 3.86 | 3.36 | 1.57 | 0.17 | 0.17 | 0.28 |
| Tb | 0.57 | 0.17 | 0.32 | 0.19 | 0.34 | 0.41 | 0.70 | 0.41 | 0.25 | 0.52 | 0.49 | 0.48 | 0.49 | 0.62 | 0.45 | 0.34 | 0.03 | 0.03 | 0.04 |
| Dy | 3.97 | 1.06 | 2.14 | 1.11 | 2.62 | 2.62 | 4.84 | 2.69 | 1.62 | 3.13 | 3.07 | 2.76 | 2.75 | 3.66 | 2.81 | 2.25 | 0.13 | 0.19 | 0.24 |
| Ho | 0.87 | 0.19 | 0.51 | 0.21 | 0.56 | 0.66 | 1.02 | 0.58 | 0.34 | 0.67 | 0.61 | 0.62 | 0.54 | 0.72 | 0.61 | 0.47 | 0.04 | 0.05 | 0.06 |
| Er | 2.59 | 0.63 | 1.40 | 0.63 | 1.59 | 1.95 | 3.04 | 1.83 | 0.86 | 1.93 | 1.81 | 1.92 | 1.72 | 2.14 | 1.68 | 1.48 | 0.11 | 0.13 | 0.23 |
| Tm | 0.38 | 0.10 | 0.21 | 0.11 | 0.24 | 0.30 | 0.44 | 0.28 | 0.11 | 0.30 | 0.28 | 0.29 | 0.30 | 0.39 | 0.28 | 0.24 | 0.02 | 0.02 | 0.03 |
| Yb | 2.55 | 0.61 | 1.49 | 0.81 | 1.66 | 1.87 | 2.59 | 1.93 | 1.02 | 1.98 | 1.90 | 1.88 | 1.77 | 2.44 | 1.85 | 1.73 | 0.09 | 0.17 | 0.26 |
| Lu | 0.37 | 0.11 | 0.23 | 0.14 | 0.26 | 0.28 | 0.41 | 0.28 | 0.15 | 0.30 | 0.32 | 0.28 | 0.26 | 0.36 | 0.32 | 0.27 | 0.01 | 0.03 | 0.04 |

| | | | | | | | | | | | | | | | | | | | |
|---|---|---|---|---|---|---|---|---|---|---|---|---|---|---|---|---|---|---|---|
| Sc | 37 | 20 | 20 | 13 | 29 | 35 | 39 | 28 | 19 | 36 | 30 | 36 | 34 | 28 | 32 | 33 | 3.02 | 0.32 | 1.23 |
| V | 297 | 157 | 171 | 110 | 220 | 261 | 265 | 233 | 123 | 313 | 216 | 256 | 270 | 215 | 237 | 237 | 1.99 | 1.88 | 3.16 |
| Mo | 0.94 | 1.37 | ud | 1.34 | ud | ud | 1.10 | 1.12 | ud | 1.71 | 2.62 | 0.83 | 2.38 | 1.51 | ud | 1.63 | 0.67 | ud | 0.53 |
| Cr | 405 | 146 | 169 | 122 | 261 | 300 | 348 | 332 | 136 | 404 | 291 | 224 | 304 | 189 | 205 | 294 | 41 | 15 | 30 |
| Co | 26 | 1.04 | 13.12 | 1.09 | 54 | 39 | 37 | 25 | 3.20 | 4.70 | 15 | 1.26 | 6.82 | 3.00 | 6.22 | 2.06 | 1.92 | 4.96 | 0.61 |
| Ni | 85 | 8 | 42 | 17 | 83 | 79 | 87 | 76 | 10 | 27 | 45 | 39 | 46 | 40 | 59 | 34 | 4.59 | 7.41 | 2.12 |
| Cu | 89 | 17 | 62 | 21 | 110 | 289 | 69 | 104 | 45 | 247 | 205 | 51 | 116 | 90 | 65 | 50 | 8 | 40 | 14 |
| Zn | 97 | 12 | 88 | 10 | 111 | 109 | 83 | 98 | 17 | 52 | 77 | 22 | 33 | 28 | 17 | 27 | 7 | 4 | 5 |
| Sn | 6.35 | 5.94 | | 10 | | | 5.54 | 4.30 | | 26 | 9.2 | 10 | 8.62 | 9.07 | | 9.75 | 2.75 | ud | 2.98 |
| W | 1.05 | 1.52 | 1.45 | 1.21 | 0.77 | 0.82 | 0.90 | 0.89 | 0.95 | 1.85 | 1.22 | 1.66 | 1.49 | 1.84 | 1.25 | 1.84 | 0.39 | 0.08 | 0.24 |
| Pb | 3.14 | 8.32 | 9.75 | 6.86 | 3.22 | 3.81 | 3.33 | 3.57 | 9.46 | 17 | 73 | 17 | 12 | 11 | 18 | 16.57 | 3.78 | 8.21 | 5.97 |
| Cd | 0.11 | 0.10 | ud | 0.12 | ud | ud | 0.11 | 0.11 | ud | 0.24 | 0.71 | 0.20 | 0.33 | 0.39 | ud | 0.30 | 0.09 | ud | 0.01 |
| Tl | 0.97 | 1.45 | 1.00 | 1.00 | 0.69 | 0.69 | 1.47 | 0.73 | 1.06 | 4.56 | 4.21 | 5.63 | 5.26 | 5.67 | 5.17 | 1.97 | 0.14 | 0.43 | 0.27 |
| Ga | 21 | 23 | 26 | 20 | 22 | 23 | 20 | 20 | 26 | 24 | 21 | 22 | 22 | 23 | 27 | 24 | 0.79 | 1.17 | 0.55 |
| As | 13 | 0.55 | 9.4 | 0.23 | 13 | 0.31 | 15 | 8.4 | 0.66 | 58 | 45 | 1.49 | 3.64 | 2.41 | 2.67 | 8.2 | 9.9 | 11.0 | 5.6 |
| Ag | 0.33 | 0.39 | 0.08 | 0.40 | ud | ud | 0.33 | 0.38 | 0.02 | 0.64 | 0.62 | 0.47 | 0.44 | 0.61 | 0.03 | 0.55 | 0.12 | 0.12 | 0.14 |
| Sb | 0.52 | 0.72 | 0.41 | 1.22 | 1.04 | 1.59 | 0.23 | 1.55 | 0.85 | 2.70 | 1.17 | 0.81 | 1.03 | 1.04 | 1.06 | 1.84 | 1.13 | 1.72 | 1.34 |
| Re | 4.49 | 3.26 | ud | 6.72 | 0.01 | ud | 8.12 | 7.40 | ud | 14.9 | 2.99 | 5.84 | 5.62 | 14.4 | ud | 2.42 | ud | ud | 1.99 |
| La/Ybn | 2.84 | 8.72 | 3.61 | 7.76 | 4.38 | 3.38 | 2.57 | 4.34 | 8.95 | 5.21 | 6.96 | 6.80 | 5.85 | 6.03 | 8.35 | 0.71 | 8.71 | 4.47 | 8.35 |
| La/Smn | 2.19 | 4.66 | 3.15 | 3.96 | 2.95 | 2.44 | 2.16 | 3.12 | 4.08 | 2.41 | 3.26 | 3.18 | 2.43 | 2.94 | 3.01 | 1.24 | 5.05 | 6.52 | 6.53 |
| Gd/Ybn | 1.05 | 1.25 | 0.99 | 1.33 | 1.12 | 1.04 | 1.23 | 1.08 | 1.45 | 1.37 | 1.44 | 1.36 | 1.45 | 1.31 | 1.50 | 0.75 | 1.56 | 0.83 | 0.89 |
| Ce/Ce* | 0.59 | 0.98 | 0.93 | 0.94 | 0.80 | 0.88 | 0.96 | 0.92 | 0.90 | 0.84 | 0.86 | 0.88 | 0.98 | 0.84 | 0.94 | 1.37 | 0.89 | 0.92 | 0.91 |
| Eu/Eu* | 0.96 | 1.26 | 1.09 | 1.03 | 0.94 | 0.91 | 0.89 | 0.89 | 0.96 | 1.05 | 0.97 | 0.98 | 0.95 | 0.91 | 0.88 | 1.38 | 1.98 | 2.45 | 2.39 |
| TREE | 58 | 35 | 42 | 40 | 51 | 51 | 64 | 62 | 59 | 84 | 90 | 89 | 87 | 103 | 107 | 20 | 5 | 5 | 12 |
| Nb/Nb* | 0.28 | 0.60 | 0.63 | 0.42 | 0.27 | 0.45 | 0.44 | 0.29 | 0.33 | 0.32 | 0.26 | 0.26 | 0.41 | 0.28 | 0.24 | 5.34 | 0.07 | 0.14 | 0.07 |
| Zr/Zr* | 1.29 | 3.79 | 2.60 | 2.67 | 1.54 | 1.62 | 1.39 | 1.40 | 1.88 | 0.93 | 1.25 | 1.09 | 1.12 | 1.24 | 0.95 | 6.29 | 0.23 | 1.62 | 0.70 |
| Hf/Hf* | 1.36 | 3.78 | 2.66 | 3.47 | 1.53 | 1.91 | 1.37 | 1.43 | 1.98 | 1.00 | 1.58 | 1.31 | 1.00 | 1.55 | 1.05 | 7.52 | 0.08 | 0.51 | 0.57 |
| Ti/Ti* | 0.83 | 1.83 | 1.08 | 1.17 | 0.89 | 0.99 | 0.70 | 0.82 | 0.91 | 0.71 | 0.58 | 0.79 | 0.75 | 0.56 | 0.66 | 1.89 | 0.31 | 0.53 | 0.25 |
| Nb/Ta | 16.0 | 13.4 | 14.2 | 13.1 | 13.9 | 16.3 | 13.9 | 14.7 | 14.2 | 14.4 | 13.3 | 17.6 | 15.9 | 12.6 | 15.8 | 14.3 | 1.4 | 10.6 | 10.0 |
| Th/Sc | 0.08 | 0.16 | 0.21 | 0.25 | 0.09 | 0.09 | 0.09 | 0.10 | 0.25 | 0.10 | 0.17 | 0.09 | 0.08 | 0.22 | 0.11 | 0.10 | 0.03 | 0.38 | 0.16 |
| Y/Ho | 25.0 | 25.6 | 22.7 | 27.2 | 20.8 | 20.2 | 24.2 | 23.7 | 22.3 | 25.4 | 25.3 | 25.3 | 27.8 | 24.2 | 23.9 | 32.7 | 34.8 | 28.3 | 33.2 |
| Th/Ce | 0.21 | 0.22 | 0.29 | 0.21 | 0.16 | 0.17 | 0.16 | 0.13 | 0.20 | 0.12 | 0.16 | 0.10 | 0.09 | 0.17 | 0.09 | 0.62 | 0.05 | 0.07 | 0.04 |
| Nb/Th | 2.07 | 2.05 | 1.54 | 1.78 | 1.79 | 2.00 | 1.65 | 1.81 | 1.44 | 1.81 | 1.52 | 2.24 | 2.55 | 1.55 | 2.08 | 2.27 | 1.75 | 2.05 | 2.00 |
| P/Nd | 131 | 0 | 87 | 0 | 131 | 131 | 131 | 87 | 437 | 131 | 175 | 0 | 0 | 87 | 437 | 44 | 0 | 437 | 0 |
| Zr/Sm | 37 | 131 | 81 | 86 | 45 | 47 | 41 | 44 | 63 | 29 | 39 | 34 | 35 | 39 | 29 | 149 | 8 | 69 | 27 |
| Hf/Sm | 1.08 | 3.59 | 2.30 | 3.09 | 1.23 | 1.54 | 1.11 | 1.24 | 1.83 | 0.87 | 1.36 | 1.12 | 0.88 | 1.34 | 0.87 | 4.92 | 0.07 | 0.60 | 0.60 |
| Cr/Th | 141 | 45 | 39 | 37 | 98 | 101 | 106 | 117 | 29 | 113 | 57 | 70 | 106 | 32 | 57 | 84 | 510 | 125 | 148 |

V, Vibhutigudda; B, Bhimangundi (Table 1).

shale and basaltic fragments in a fine-grained Fe–Mg rich matrix of greywackes substantiates this inference (Manikyamba et al., 1997a).

Population II greywackes plot to lower Sc content on the mixing hyperbolae between Archean TTG and tholeiitic basalt endmembers in diagrams of Th/Sc vs Sc, whereas shales of this study cluster near the basalt endmember (Fig. 5). The compositional variations, and stratigraphic association, can be reconciled in a transgression-regression scenario. During pronounced transgressions, deep water and shore-distal conditions prevail; the LKS-MKS arc is the dominant catchment for fine-grained shales in a forearc trench or back-arc. During mild regressions, high energy Type I, arc-dominated, greywacke facies are deposited, whereas during pronounced regressions the felsic catchment predominates (Fig. 5).

### 6.3. Eu anomalies

First cycle volcanogenic turbidites internal to Archean greenstone belts have no or minor positive Eu anomalies. They are interpreted to have been shed off bimodal arc basalts and dacites/tonalities into forearc trenches. Arc basalts have no Eu anomalies and the dacites/tonalites have zero to positive Eu anomalies from variable accumulation of plagioclase, whereas intracrustal granite melts are characterized by negative Eu anomalies (Taylor and McLennan, 1985, 1995; McLennan and Taylor, 1991). According to Condie (1993), the size of Eu anomaly is greater in Archaean cratonic shales ($Eu/Eu^* = 0.73$) compared with Proterozoic shales (0.66). Similarly, Gao and Wedepohl (1995) reported negative Eu anomalies in Archean cratonic shales. Greywackes, Archean and younger, exhibit negative Eu anomalies as a result of a continental terrigenous contribution (Taylor and McLennan, 1981; Naqvi et al., 1983, 1988; Condie, 1993).

Sandur shales exhibit both negative and positive anomalies ($Eu/Eu^* = 0.88$–$1.38$; Table 3). Given their compositional similarity to arc basalts, that have no or minor Eu anomalies, but a stratigraphic association with cherts having positive Eu anomalies, the range of Eu anomalies is interpreted to stem from leaching or precipitation of $Eu^{2+}$ (Humphries, 1984).

### 6.4. Zr–Hf anomalies

Five samples of shales possess variably high Zr/Sm ratios of 63–149 (Fig. 6). Primitive mantle has a ratio of 25, Archaean upper continental crust 31, PAAS is 38, and most magmatic zircons are in the range 25–60 (Taylor and McLennan, 1985, 1995; Sun and McDonough, 1989; Rudnick and Gao, 2004). Taylor and McLennan (1985) noted that some of the HFSE might be fractionated during sedimentary processes due to their residence in heavy minerals, but that any such effects are minimal in fine-grained facies. Plank and Langmuir (1998) suggested that marine sediments provide a reliable estimate of average composition of the upper continental crust (Nb, Ta, and Ti excepted) as oceanic proceses are unlikely to fractionate the REE and HFSE.

Zr–Hf anomalies could reflect detrital accumulations of zircon. However, an arc basalt dominated catchment would not have been a source of zircons, and heavy mineral accumulation in fine-grained facies is unlikely especially given that the troughs at Nb–Ta likely indicate winnowing out of a titanite in higher energy facies (Fig. 3). The peaks at Zr–Hf could also be inherited from erosion of underlying greywackes which also feature Zr anomalies (Manikyamba et al., 1997a). That too is unlikely, given that greywackes plot on mixing lines between basalt and TTG endmembers, but population I shales do not (Fig. 5).

Taylor and McLennan (1985, 1995) reported positive normalized Zr anomalies in loess due to the aerodynamic properties of zircon. Ratios of Zr/Hf in these shales span 29 to 47 compared to the AUCC value of 31. That scatter, taken with the shales plotting near the arc endmember, signify that airborne input from a cratonic, zircon bearing, source is improbable (Figs. 4 and 5).

The conjunction of normalized HREE enrichment and fractionation, with fractionations of Zr, Hf/ MREE, and of Zr/Hf, have been reported from magadiitic cherts of the East African Rift and diagenetically altered siltstones of the ~1.4 Ga Belt-Purcell Supergroup, North America, both of which involved alkaline oxidizing brines (Kerrich et al., 2002; Gonzalez-Alvarez et al., 2006). The most extreme Zr/Sm ratios in five samples occur at variably fractionated HREE relative to the coherent group of eleven shales (Fig. 5). Accordingly, the Zr/Sm anomalies >60 are attributed to hydrothermal alteration, and small variable anomalies in the remaining shales to subdued metasomatism.

### 6.5. Hydrothermal gains and losses

Algoma type Archean BIF-chert are generally deposited during periods of quiescence between active volcanism of Archaean greenstone belts (Fryer et al., 1979; Simonson and Hassler, 1996; Kerr, 1998; Ohmoto, 2004; Trendall and Blockley, 2004). The BIF of the Dharwar, Superior, and other cratons are locally interbedded with volcanic flows or aluminous–ferruginous shales. Their major element, REE and trace element abundances indicate their derivation as a volcaniclastic component mixed with hydrothermal precipitates, dominantly $SiO_2$ and $Fe_2O_3$ (Trendall, 1983; Dymek and Klein, 1988; Jacobsen and Pimentel-Klose, 1988; Derry and Jacobsen, 1990; Gross, 1991; Manikyamba et al., 1993; Arora et al., 1995; Gnaneshwar Rao and Naqvi, 1995; Khan and Naqvi, 1996).

Cherts of the Sandur Superterrane are likewise interpreted to be hydrothermal precipitates deposited during periods of quiescence between volcanic cycles. Compositionally, they are dominated by silica, with positive Eu anomalies indicative of reducing hydrothermal fluids

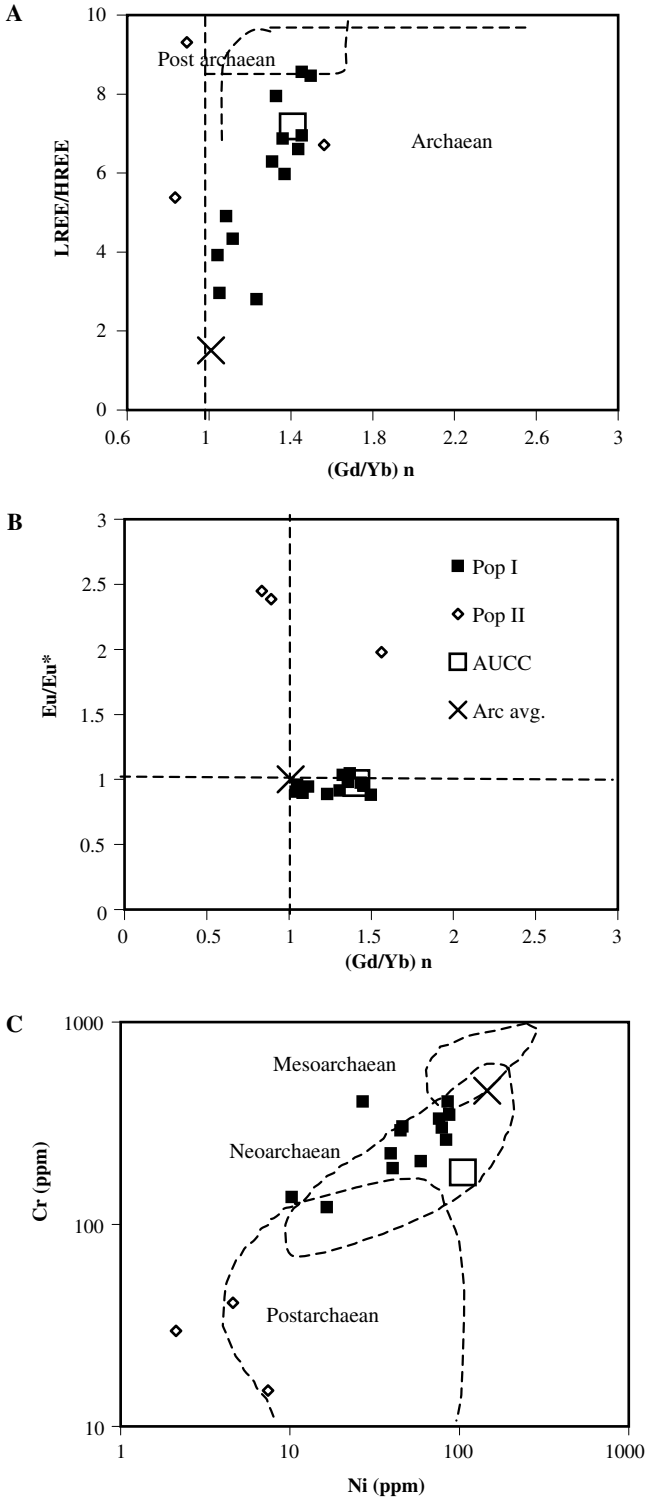


Fig. 4. Diagram of LREE/HREE vs $Gd/Yb_n$ (A), and $Eu/Eu^*$ vs $Gd/Yb_n$ (B) after Taylor and McLennan (1985); Ni vs Cr (C) after Condie (1993); arc average after Manikyamba et al. (2004).

(Humphries, 1984). The presence of variable proportions of carbonaceous compounds in both shales and black cherts endorses deposition under reducing conditions (Kerrich et al., 2006). These samples are similar to the ferruginous cherts which are found to the west of Bhimang-

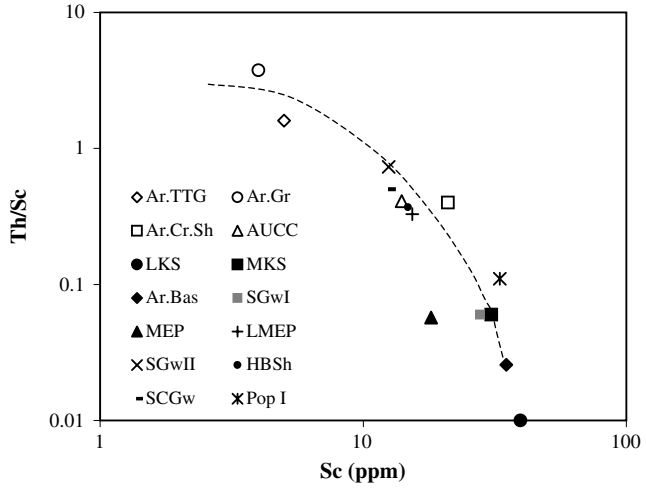


Fig. 5. Plot of Th/Sc vs Sc (after Bhat and Ghosh, 2001). Ar. TTG—Archean TTG, Ar, Gr—Archean granite, Ar. Bas—Archean basalt, Ar. Cr.Sh—Archean cratonic shale, from Condie (1993). LKS—and HKS—, respectively low- and medium-K Archean intraoceanic arc tholeiitic basalt series (Hollings and Kerrich, 2006). S Gw I and S Gw II, Sandur Types I and II greywackes from Manikyamba et al. (1997a). MEP and LMEP, respectively mafic- and low-mafic element populations from the 2.7 Ga Abitibi greenstone terrane (Feng and Kerrich, 1990; Feng et al., 1993). HBSh and SCGw, shales and greywacke averages from the Neoarchean Wawa greenstone terrane (Polat et al., 1998).

undi (Manikyamba et al., 1993). They bear the signature of primary hydrothermal fluids added to the ambient ocean at the vents of the volcanic-hydrothermal fields on or near plume basalts (Manikyamba et al., 1993), or arcs in the case of this study.

The inferred hydrothermal activity may also have influenced the shales. Depletions of MgO, CaO, and $Na_2O$ may reflect weathering of the arc catchment (Fedo et al., 1995; Nesbitt and Young, 2004). However, those losses, together with variability of Si, and Fe, and "gains of K" in the population I shale average, relative to AUCC, are most plausibly the result of hydrothermal activity, given the context of stratigraphically associated cherts (Fig. 6). That interpretation accounts for the shales being aluminous relative to "Archaean unaltered" tholeiitic arc basalts (Hollings and Kerrich, 2004, 2006; Manikyamba et al., 2004).

## 7. Implications and conclusions

The Neoarchaean is characterized by a peak of mantle plume activity, reflected in continental and oceanic large igneous provinces (LIPs). According to Isley and Abbott (1999) and Condie et al. (2001), mantle plumes, LIPs, BIF, the chemical weathering index of alteration of shales (CIA), black shales and the ratio of black shale/total shale have common time series, all with peaks at 2.7 Ga. Wyman and coworkers have also documented from field relationships and geochemistry that komatiite–basalt sequences, likely erupted from mantle plumes and representing ocean plateaus, and arc-basalt volcanic sequences erupted coevally and proximal to each other in several Neoarchean greenstone terranes. Those relationships were interpreted

Table 4
Correlation matrix for population I shales (excluding **C-5,15,17,22,23**)

| | $SiO_2$ | $TiO_2$ | $Al_2O_3$ | $Fe_2O_3$ | MgO | $K_2O$ | $Na_2O$ | Mg# | Rb | Cs | Ba | Cr | Co | Ni | Sc | V | Nb | Zr | Hf | Th | Y | La | Ce | Eu | Gd | Yb |
|---|---|---|---|---|---|---|---|---|---|---|---|---|---|---|---|---|---|---|---|---|---|---|---|---|---|---|
| $SiO_2$ | 1.00 | | | | | | | | | | | | | | | | | | | | | | | | | |
| $TiO_2$ | 0.39 | 1.00 | | | | | | | | | | | | | | | | | | | | | | | | |
| $Al_2O_3$ | 0.22 | 0.54 | 1.00 | | | | | | | | | | | | | | | | | | | | | | | |
| $Fe_2O_3$ | −0.86 | −0.58 | −0.65 | 1.00 | | | | | | | | | | | | | | | | | | | | | | |
| MgO | −0.87 | −0.42 | −0.28 | 0.73 | 1.00 | | | | | | | | | | | | | | | | | | | | | |
| $K_2O$ | 0.24 | 0.47 | 0.56 | −0.48 | −0.33 | 1.00 | | | | | | | | | | | | | | | | | | | | |
| $Na_2O$ | 0.84 | 0.50 | 0.50 | −0.81 | −0.96 | 0.38 | 1.00 | | | | | | | | | | | | | | | | | | | |
| Mg# | −0.64 | −0.24 | −0.08 | 0.40 | 0.90 | −0.14 | −0.83 | 1.00 | | | | | | | | | | | | | | | | | | |
| Rb | −0.31 | 0.18 | 0.30 | 0.02 | 0.25 | 0.68 | −0.21 | 0.37 | 1.00 | | | | | | | | | | | | | | | | | |
| Cs | −0.01 | 0.17 | 0.31 | −0.22 | 0.00 | 0.59 | 0.03 | 0.19 | 0.89 | 1.00 | | | | | | | | | | | | | | | | |
| Ba | 0.77 | 0.46 | 0.66 | −0.87 | −0.84 | 0.56 | 0.92 | −0.63 | 0.10 | 0.35 | 1.00 | | | | | | | | | | | | | | | |
| Cr | −0.58 | −0.01 | −0.55 | 0.71 | 0.41 | −0.03 | −0.53 | 0.17 | 0.23 | −0.02 | −0.63 | 1.00 | | | | | | | | | | | | | | |
| Co | −0.78 | −0.60 | −0.40 | 0.74 | 0.88 | −0.40 | −0.90 | 0.75 | 0.19 | −0.04 | −0.79 | 0.25 | 1.00 | | | | | | | | | | | | | |
| Ni | −0.80 | −0.36 | −0.06 | 0.57 | 0.90 | −0.05 | −0.84 | 0.85 | 0.42 | 0.13 | −0.65 | 0.25 | 0.86 | 1.00 | | | | | | | | | | | | |
| Sc | −0.19 | 0.62 | 0.09 | 0.04 | 0.08 | 0.44 | −0.10 | 0.16 | 0.56 | 0.34 | −0.12 | 0.52 | −0.01 | 0.12 | 1.00 | | | | | | | | | | | |
| V | −0.18 | 0.61 | −0.17 | 0.19 | 0.07 | 0.16 | −0.13 | 0.01 | 0.25 | 0.07 | −0.25 | 0.75 | −0.12 | −0.07 | 0.81 | 1.00 | | | | | | | | | | |
| Nb | 0.64 | 0.36 | 0.64 | −0.71 | −0.83 | 0.35 | 0.92 | −0.75 | −0.14 | 0.08 | 0.90 | −0.57 | −0.79 | −0.73 | −0.23 | −0.26 | 1.00 | | | | | | | | | |
| Zr | 0.53 | 0.17 | 0.63 | −0.61 | −0.72 | 0.38 | 0.82 | −0.68 | −0.10 | 0.07 | 0.84 | −0.58 | −0.66 | −0.59 | −0.36 | −0.41 | 0.96 | 1.00 | | | | | | | | |
| Hf | 0.44 | 0.05 | 0.56 | −0.53 | −0.62 | 0.23 | 0.73 | −0.56 | −0.04 | 0.23 | 0.79 | −0.60 | −0.58 | −0.57 | −0.41 | −0.47 | 0.91 | 0.93 | 1.00 | | | | | | | |
| Th | 0.37 | −0.13 | 0.36 | −0.37 | −0.58 | 0.25 | 0.63 | −0.61 | 0.03 | 0.29 | 0.71 | −0.45 | −0.48 | −0.53 | −0.44 | −0.46 | 0.81 | 0.88 | 0.94 | 1.00 | | | | | | |
| Y | −0.24 | 0.27 | 0.22 | 0.05 | 0.05 | 0.80 | −0.04 | 0.08 | 0.87 | 0.68 | 0.13 | 0.45 | −0.03 | 0.19 | 0.64 | 0.45 | −0.01 | 0.04 | −0.01 | 0.10 | 1.00 | | | | | |
| La | 0.82 | 0.29 | 0.48 | −0.79 | −0.87 | 0.28 | 0.91 | −0.73 | −0.21 | 0.12 | 0.91 | −0.67 | −0.81 | −0.73 | −0.36 | −0.39 | 0.87 | 0.79 | 0.77 | 0.69 | −0.20 | 1.00 | | | | |
| Ce | 0.88 | 0.37 | 0.43 | −0.83 | −0.93 | 0.31 | 0.93 | −0.78 | −0.29 | 0.00 | 0.85 | −0.61 | −0.84 | −0.77 | −0.23 | −0.27 | 0.82 | 0.73 | 0.63 | 0.55 | −0.20 | 0.94 | 1.00 | | | |
| Eu | 0.70 | 0.55 | 0.39 | −0.65 | −0.91 | 0.53 | 0.90 | −0.85 | 0.06 | 0.25 | 0.86 | −0.20 | −0.87 | −0.80 | 0.09 | 0.14 | 0.82 | 0.73 | 0.63 | 0.64 | 0.28 | 0.79 | 0.79 | 1.00 | | |
| Gd | 0.36 | 0.37 | 0.47 | −0.47 | −0.58 | 0.87 | 0.59 | −0.50 | 0.56 | 0.59 | 0.72 | −0.06 | −0.55 | −0.36 | 0.27 | 0.11 | 0.60 | 0.63 | 0.53 | 0.61 | 0.73 | 0.48 | 0.48 | 0.79 | 1.00 | |
| Yb | −0.30 | 0.16 | 0.36 | 0.03 | 0.14 | 0.72 | −0.07 | 0.16 | 0.84 | 0.70 | 0.19 | 0.29 | 0.00 | 0.24 | 0.36 | 0.25 | 0.10 | 0.20 | 0.19 | 0.29 | 0.91 | −0.14 | −0.23 | 0.22 | 0.69 | 1.00 |

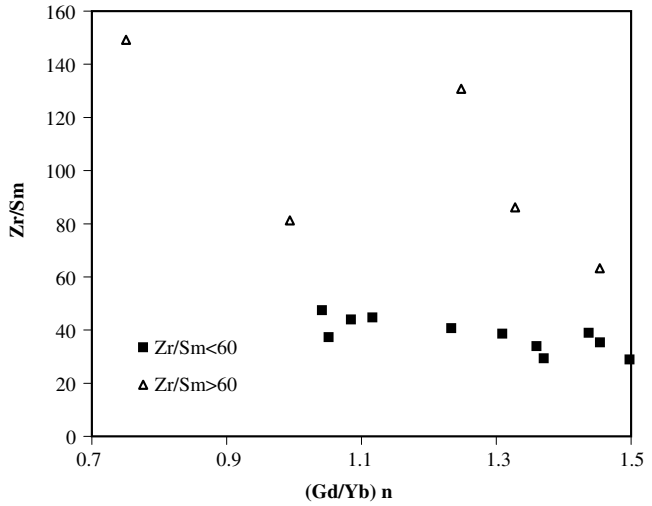


Fig. 6. Plot of Zr/Sm versus $Gd/Yb_n$ illustrating the coherent behaviour of eleven samples, but scatter of five.

as migrating arcs being captured by, and jammed by, ocean plateaus (Hollings and Wyman, 1999; Polat et al., 1999; Wyman et al., 1999; Kerrich et al., 2000), as is presently occurring for the Ontong-Java plateau and New Ireland arc (MacInnes et al., 1999).

Taylor and McLennan (1985, 1995) have shown that first cycle volcanogenic turbidites of Archean greenstone terranes plot on mixing hyperbolae between bimodal arc magmas. Arc basalt is the mafic (high Sc, low Th) endmember, and dacite volcanics, or tonalite intrusive counterparts, the felsic (low Sc, high Th) endmember devoid of negative Eu anomalies. In contrast, Archean cratonic shales, likely deposited on passive magins, have composite signatures: fractionated REE with negative Eu anomalies of granitic terranes, and relatively high Cr, Ni contents of eroded komatiite–basalt volcanic sequences (Naqvi et al., 1983, 1988; Wronkiewicz and Condie, 1987, 1989; Condie, 1993; Gao and Wedepohl, 1995).

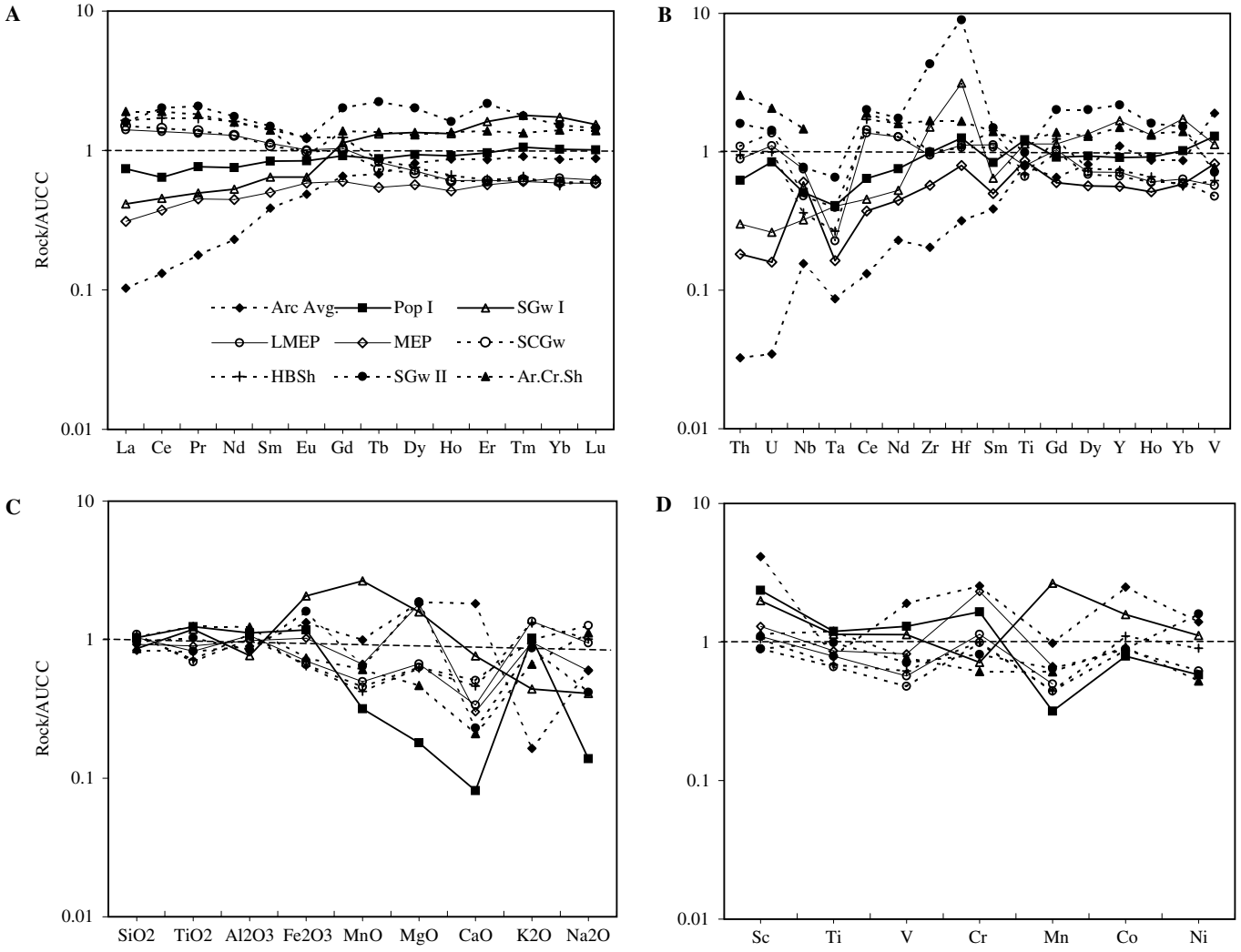


Fig. 7. Plots of REE (A), multielements (B), major elements (C), and transition elements (D) for specified average Archean sedimentary rock compositions, normalized to Average upper crustal compositions of Taylor and McLennan (1985). Sources: 1- Sandur shale population I (Pop I) (Table 3); 2, 3 Sandur greywackes Types I and II (S Gw I, II) respectively, after Manikyamba et al. (1997a); 4, 5- mafic- (MEP) and low mafic-element populations (LMEP) from the 2.7 Ga Abitibi composite greenstone terrane (Feng and Kerrich, 1990; Feng et al., 1993); 6,7- Heron Bay shale (HB Sh) and Schreiber greywacke (SC Gw) averages from the 2.7 Ga Wawa greenstone terrane (Polat et al., 1998) and arc average from Manikyamba et al. (2004).

Black shales from the Sandur Superterrane constitute a mafic endmember, being trench turbidites with a provenance in an intraoceanic arc dominated by LKS- and MKS- basalts. Consequently, the catchment was a unimodal arc devoid of cratonic input, rather than the bimodal source of Taylor and McLennan (1985, 1995). Modern counterparts would be trenches paired to the South Sandwich or LKS sectors of the Lesser Antilles arcs (Hawkesworth et al., 1993; Macdonald et al., 2000). Greywackes underlying Sandur black shales show two provenances. Type I, compositionally similar to black shale population I of this study, and Type II having a cratonic signature. Collectively, the results are interpreted in terms of an oceanic arc near a continental margin. During transgressions the basin is fed by the arc, whereas during regression the basin receives detritus from a continental catchment.

Sandstones and shales of the 2.7 Ga Wawa greenstone terrane, Superior Province, plot close to AUCC on the Th/Sc vs Sc mixing hyperbola, and at ~1 on AUCC-normalized diagrams, indicative of a bimodal arc provenance (Figs. 5 and 7). Similarly, the low mafic element population (LMEP) turbidites of the 2.7 Ga Abitibi greenstone terrane have a bimodal arc signature, whereas mafic element population (MEP) turbidites having high Cr, Co, and Ni-contents likely represent fans shed off komatiite–basalt dominated ocean plateaus (Figs. 5 and 7; Feng et al., 1993).

In summary, the composition of these first cycle intraoceanic volcanogenic black shales provide additional constraints on the geodynamic processes controlling the lithotectonic associations of the eastern volcanic and eastern felsic volcanic terranes of the Neoarchean Sandur Superterrane. A typical Archean intraoceanic arc, or back-arc, distal to an active continental margin. In contrast, the slighty younger 2.5 Ga Rampur group pelites of western Himalaya have highly fractionated REE patterns with $La/Yb_n$ ranging from 8.8–18.6 exhibiting negative Eu anomalies ($Eu/Eu^* = 0.69–0.56$). These pelites are much closer in composition with Proterozoic shale composition. Bhat and Ghosh (2001) interpreted the dominant source was a gneissic complex present in the northern Indian craton.

## Acknowledgments

R. Kerrich acknowledges funding from an NSERC Discovery Grant, an NSERC MFA grant partially to support the ICP-MS lab, as well as the George McLeod endowment to the Department of Geological Sciences. CM is thankful to Dr. V.P. Dimri, Director, NGRI for permission to publish this work. We are grateful to Dr. Ken Sugitani and an anonymous Journal reviewer, as well as Dr. Goldhaber the Associate Editor, for their critical reviews which have significantly improved the manuscript. We are grateful to Dr. J. Fan for ICP-MS analyses. C.M. thanks Dr. S.M. Naqvi for his constant support and encouragement to carry out this work, to Dr. M. Ram Mohan for his help in the field work, and Mr. Tarun C. Khanna for processing the data.

*Associate editor:* Martin B. Goldhaber

## Appendix A

| | Ar.TTG* | Ar.Gr | Ar.Bas | Ar.Cr.Sh | AUCC | LKS | MKS | S Gw I | S Gw II | MEP | LMEP | HBSh | SCGw | Arc avg. | Pop I |
|---|---|---|---|---|---|---|---|---|---|---|---|---|---|---|---|
| $SiO_2$ | 69.50 | 72.40 | 50.50 | 60.95 | 60.10 | 48.15 | 53.22 | 51.78 | 58.12 | 55.50 | 62.10 | 64.65 | 65.74 | 50.43 | 62.32 |
| $TiO_2$ | 0.34 | 0.25 | 0.99 | 0.62 | 0.80 | 0.97 | 1.81 | 0.95 | 0.82 | 0.72 | 0.66 | 0.57 | 0.55 | 0.66 | 0.99 |
| $Al_2O_3$ | 15.10 | 14.80 | 15.30 | 17.50 | 15.30 | 15.57 | 12.58 | 11.77 | 12.97 | 15.10 | 16.40 | 16.83 | 15.55 | 13.76 | 17.16 |
| FeO (t) | 3.50 | 1.94 | 10.20 | 7.53 | 8.00 | | | | | | | | | | |
| | | | | | 17.13 | 17.52 | 18.19 | 14.11 | 9.01 | 6.18 | 5.69 | 5.83 | 11.72 | 10.33 | |
| MgO | 1.10 | 0.37 | 9.40 | 3.88 | 4.70 | 7.45 | 3.67 | 7.46 | 8.81 | 8.51 | 3.15 | 2.92 | 2.97 | 8.81 | 0.85 |
| CaO | 2.80 | 1.18 | 10.00 | 0.64 | 6.20 | 10.20 | 7.32 | 4.74 | 1.43 | 1.87 | 2.10 | 2.87 | 3.15 | 11.28 | 0.50 |
| $Na_2O$ | 4.50 | 3.16 | 2.40 | 0.68 | 3.00 | 2.46 | 2.86 | 1.35 | 1.38 | 1.97 | 3.12 | 3.33 | 4.17 | 1.99 | 0.46 |
| $K_2O$ | 2.40 | 4.94 | 0.43 | 3.07 | 0.90 | 0.69 | 0.49 | 0.79 | 1.57 | 1.72 | 2.44 | 2.37 | 1.79 | 0.30 | 1.84 |
| $P_2O_5$ | 0.11 | 0.08 | 0.11 | 0.10 | — | 0.06 | 0.27 | 0.08 | 0.25 | 0.10 | 0.16 | 0.21 | 0.15 | 0.05 | 0.03 |
| Rb | 65 | 150 | 12 | 111 | 50 | 9 | 11 | 30 | 30 | 40 | 66 | 59 | 58 | 12.83 | 97 |
| Sr | 435 | 145 | 132 | 61 | 240 | 162 | 141 | 88 | 73 | 85 | 294 | 700 | 524 | 131 | 71 |
| Ba | 660 | 765 | 147 | 456 | 265 | 94 | 84 | 134 | 200 | 215 | 631 | 703 | 545 | 43 | 181 |
| Pb | 19 | 25 | 5 | 13 | | — | — | 23 | 10 | 2 | 10 | — | — | | 15 |
| Th | 8.00 | 15.00 | 1.00 | 8.50 | 5.70 | 0.45 | 1.82 | 1.72 | 9.14 | 1.04 | 5.06 | 5.41 | 6.23 | 0.19 | 3.54 |
| U | 2.00 | 3.50 | 1.00 | 2.40 | 1.50 | 0.10 | 0.45 | 0.39 | 2.14 | 0.24 | 1.66 | 1.50 | 2.05 | 0.03 | 1.27 |
| Zr | 160 | 155 | 82 | 151 | 125 | 53 | 181 | 189 | 539 | 72 | 118 | 122 | 126 | 25 | 124 |
| Hf | 4.00 | 4.50 | 2.20 | 4.50 | 3.00 | 1.57 | 5.06 | 9.40 | 26.97 | 2.39 | 3.35 | 3.26 | 3.23 | 0.95 | 3.77 |
| Nb | 8 | 12 | 6 | 11 | 13 | 3 | 10 | 4 | 10 | 8 | 10 | 5 | 6 | 2 | 7 |
| Ta | 0.70 | 1.00 | 0.30 | 0.84 | 1.10 | 0.20 | 0.62 | 0.45 | 0.72 | 0.18 | 0.25 | 0.29 | 0.44 | 0.10 | 0.45 |
| Y | 13 | 20 | 20 | 28 | 18 | 17 | 53 | 30 | 39 | 10 | 13 | 13 | 12 | 20 | 16 |
| La | 30 | 50 | 8 | 31 | 20 | 4 | 15 | 8 | 32 | 6 | 28 | 33 | 30 | 2 | 15 |
| Ce | 56 | 95 | 19 | 61 | 42 | 11 | 36 | 19 | 85 | 16 | 58 | 72 | 61 | 6 | 27 |
| Nd | 22 | 46 | 11 | 28 | 20 | 8 | 24 | 11 | 35 | 9 | 26 | 32 | 26 | 5 | 15 |
| Sm | 3 | 6 | 3 | 5 | 4 | 1 | 2 | 3 | 6 | 2 | 5 | 6 | 4 | 2 | 3 |
| Eu | 1.00 | 0.85 | 1.00 | 1.12 | 1.20 | — | — | 0.77 | 1.46 | 0.70 | 1.21 | 1.48 | 1.18 | 0.58 | 1.01 |
| Gd | 2.98 | 4.60 | 3.26 | 4.55 | 3.40 | 3.01 | 3.68 | 3.87 | 6.86 | 2.04 | 3.51 | 4.22 | 3.40 | 2.23 | 3.11 |
| Tb | 0.45 | 0.65 | 0.55 | 0.71 | 0.57 | 0.48 | 1.44 | 0.75 | 1.27 | 0.31 | 0.47 | 0.49 | 0.42 | 0.39 | 0.50 |
| Yb | 1.00 | 2.00 | 2.30 | 2.43 | 2.00 | 1.62 | 5.67 | 3.47 | 3.04 | 1.17 | 1.27 | 1.13 | 1.20 | 1.73 | 2.04 |
| Lu | 0.17 | 0.32 | 0.38 | 0.39 | 0.31 | 0.25 | 0.85 | 0.48 | 0.45 | 0.18 | 0.19 | 0.19 | 0.18 | 0.27 | 0.31 |
| Sc | 5 | 4 | 37 | 21 | 14 | 40 | 31 | 28 | 13 | 18 | 15 | 15 | 13 | 58 | 33 |
| V | 37 | 15 | 240 | 154 | 195 | 261 | 222 | 220 | 139 | 160 | 111 | 121 | 93 | 371 | 253 |
| Cr | 22 | 16 | 456 | 507 | 180 | 280 | 15 | 129 | 147 | 417 | 205 | 181 | 178 | 457 | 297 |
| Co | 10 | 4 | 59 | 31 | 25 | 75 | 46 | 39 | 22 | — | — | 28 | 22 | 62 | 20 |
| Ni | 13 | 12 | 190 | 221 | 105 | 192 | 24 | 117 | 167 | | — | 95 | 65 | 146 | 61 |
| Eu/Eu* | 0.97 | 0.48 | 0.98 | 0.73 | 0.97 | | — | 0.74 | 0.70 | 1.06 | 0.93 | 0.88 | 0.91 | 1.00 | 0.94 |
| $(La/Yb)_n$ | 18.2 | 15.2 | 2 | 7.7 | 7.2 | 1.8 | 1.9 | 1.7 | 7.5 | 3.5 | 15 | 20.8 | 18.0 | 0.82 | 5.16 |

* Abbreviations as in caption to Fig. 5.

## References


Arora, M., Khan, R.M.K., Naqvi, S.M., 1994. Composition of the middle and late Archaean upper continental crust as sampled from the Kaldurga Conglomerate, Dharwar craton, India. *Precambrian Res.* **70**, 93–112.

Arora, M., Govil, P.K., Charan, S.N., Uday Raj, B., Manikyamba, C., Chatterjee, A.K., Naqvi, S.M., 1995. Geochemistry and origin of Archaean banded iron-formation from the Bababudan schist belt, India. *Econ. Geol.* **90**, 2040–2057.

Bhat, M.I., Ghosh, S.K., 2001. Geochemistry of the 2.51 Ga Old Rampur group pelites, western Himalayas: implications for their provenance and weathering. *Precambrian Res.* **108**, 1–16.

Chadwick, B., Vasudev, V.N., Ahmad, N., 1996. The Sandur schist belt and its adjacent plutonic rocks: implications for late Archaean crustal evolution in Karnataka. *J. Geol. Soc. Ind.* **47**, 37–57.

Condie, K.C., Wilks, M., Rosen, D.M., Zlobin, V.L., 1991. Geochemistry of metasediments from the Precambrian Hapschan Series, eastern Anabar Shield, Siberia. *Precambrian Res.* **50**, 37–47.

Condie, K.C., 1993. Chemical composition and evolution of the upper continental crust: contrasting results from surface samples and shales. *Chem. Geol.* **104**, 1–37.

Condie, K.C., Des Marais, D.J., Abbott, D., 2001. Precambrian superplumes and supercontinents: a record in black shales, carbon isotopes, and paleoclimates? *Precambrian Res.* **106**, 239–260.

Derry, L.A., Jacobsen, S.B., 1990. The chemical evolution of Precambrian seawater: evidence from REEs in banded iron formations. *Geochim. Cosmochim. Acta* **54**, 2965–2977.

Dymek, R.F., Klein, C., 1988. Chemistry, petrology and origin of banded iron formation lithologies from the 3800 Ma Isua supracrustal belt, West Greenland. *Precambrian Res.* **39**, 247–302.

Fan, J., Kerrich, R., 1997. Geochemical characteristics of Al-depleted and undepleted komatiites and HREE-enriched tholeiites, western Abitibi greenstone belt: variable HFSE/REE systematicsin a heterogeneous mantle plume. *Geochim. Cosmochim. Acta* **61**, 4723–4744.

Fedo, C.M., Nesbitt, H.W., Young, G.M., 1995. Unraveling the effects of potassium metasomatism in sedimentary rocks and paleosols, with implications for paleoweathering conditions and provenance. *Geology* **23** (10), 921–924.

Feng, R., Kerrich, R., 1990. Geochemistry of fine-grained clastic sediments in the Archaean Abitibi greenstone belt, Canada: implications for provenance and tectonic setting. *Geochim. Cosmochim. Acta* **54**, 1061–1081.

Feng, R., Kerrich, R., Maas, R., 1993. Geochemical, oxygen and neodymium isotope compositions of metasedimens from the Abitibi greenstone belt and Pontaic Subprovince, Canada: evidence for ancient crust and Archaean terrane juxtaposition. *Geochim. Cosmochim. Acta* **57**, 641–658.

Fryer, B.J., Fyfe, W.S., Kerrich, R., 1979. Archaean volcanogenic oceans. *Chem. Geol.* **24**, 25–33.

Gao, S., Wedepohl, K.H., 1995. The negative Eu anomaly in Archaean sedimentary rocks: implications for decomposition, age and importance of their granitic sources. *Earth Planet. Sci. Lett.* **133**, 81–94.

Gao, S., Liu, X., Yuan, H., Hatterndorf, B., Gunther, D., Chen, L., Hu, S., 2002. Determination of forty two major and trace elements in USGS and NIST SRM glasses by laser ablation-inductively coupled plasma-mass spectrometry. *Geostand. Newslett.* **26**, 181–196.

Gibbs, A.K., Montgomery, C.W., O'Day, P.A., Erslev, E.A., 1986. The Archaean-Proterozoic transition: evidence from the geochemistry of metasedimentary rocks of Guyana and Montana. *Geochim. Cosmochim. Acta* **50**, 2125–2141.

Gonzalez-Alvarez, I.J., Kusiak, M.A., Kerrich, R., 2006. A trace element and chemical Th–U total Pb dating study in the lower belt-Purcell Supergroup, western north America: provenance and diagenetic implications. *Chem. Geol.* **230**, 140–160.

Gross, G.A., 1991. Genetic concepts for iron formation and associaitemed metalliferous sediments. *Econ. Geol. Monogr.* **81**, 51–88.

Gnaneshwar Rao, T., Naqvi, S.M., 1995. Geochemistry, depositional environment and tectonic setting of the BIF's of the Late Archaean Chitradurga Schist Belt, India. *Chem. Geol.* **121**, 217–243.

Hawkesworth, C.J., Gallagher, K., Hergt, J.M., McDermott, F., 1993. Mantle and slab contribution in arc magmas. *Annu. Rev. Earth Planet. Sci.* **21**, 175–204.

Holland, D.H., 1978. *The chemistry of the atmosphere and oceans*. Wiley and Sons, New York, USA.

Hollings, P., Wyman, D.A., 1999. Trace element and Sm–Nd systematics of volcanic and intrusive rocks from the 3 Ga Lumby Lake greenstone belt, Superior Province: evidence for Archaean plume-arc interaction. *Lithos* **46**, 189–213.

Hollings, P., Kerrich, R., 2004. Geochemical systematics of tholeiites from the 2.86 Ga Pickle Crow assemblage, northwestern Ontario: arc basalts with positive and negative Nb–Hf anomalies. *Precambrian Res.* **134**, 1–20.

Hollings, P., Kerrich, R., 2006. Light rare earth element depleted to enriched basaltic flows from 2.8 to 2.7 Ga greenstone belts of the Uchi Subprovince, Ontario, Canada. *Chem. Geol.* **227**, 133–153.

Humphries, S.E., 1984. The mobility of rare earth elements in the crust. In: Henderson, P. (Ed.), *Rare Earth Element Geochemistry*. Elsevier, Oxford, pp. 317–342.

Isley, A.E., Abbott, D.H., 1999. Plume-related mafic volcanism and the deposition of banded iron formation. *J. Geophy. Res.* **104**, 15461–15477.

Jackson, S.L., Fyon, J.A., 1991. The western Abitibi subprovince in Ontario. In: Thurston, P.C. (Ed.), *Geology of Ontario*, Ontario Geol. Surv. Spec., vol. 4, pp. 405–484.

Jacobsen, S.B., Pimentel-Klose, M.R., 1988. A Nd isotopic study of the Hamersley and Michipicoten banded iron formations: the source of REE and Fe in Archaean oceans. *Earth Planet. Sci. Lett.* **87**, 29–44.

Kerr, A.C., 1998. Oceanic Plateau formation: a cause of mass extinction and black shale deposition around the Cenomanian–Turonian boundary? *J. Geol. Soc.* **115**, 619–626.

Kerrich, R., Xie, Q., 2002. Compositional recycling structure of an Archaean Super-plume: Nb–Th–U-LREE systematics of Archaean komatiites and basalts revisited. *Contrib. Mineral. Petrol.* **142**, 476–484.

Kerrich, R., Goldfarb, R., Groves, D., Garwin, S., Jia, Y., 2000. The characteristics, origins and geodynamic settings of supergaint gold metallogenic provinces, Science in China. *Earth Sci.* **43**, 1–68.

Kerrich, R., Renaut, R.W., Bonli, T., 2002. Trace element composition of cherts from alkaline lakes in east African rift: a probe for ancient counter parts. In: Renaut, R.W., Ashley, G.M. (Eds.), *Sedimentation in Continental Rifts*, Soc. Sed. Geol., Boulder, Colorodo, Spe. Publ., 73, pp. 277–298.

Kerrich, R., Jia, Y., Manikyamba, C., Naqvi, S.M., 2006. Secular variation of N-isotopes in terrestrial reservoirs and ore deposits. *Spe. Publ. Geol. Soc. Am.* **198** (in press).

Khan, R.M.K., Naqvi, S.M., 1996. Geology, geochemistry and genesis of BIF of Kushtagi Schist Belt, Archaean Dharwar Craton, India. *Mineral. Deposita* **31**, 123–133.

Macdonald, R., Hawkesworth, C.J., Heath, E., 2000. The Lesser Antilles volcanic chain a study in arc magmatism. *Earth Sci. Rev.* **49**, 1–76.

MacInnes, B.I.A., McBride, J.S., Evans, N.J., Lambert, D.D., Andrew, A.S., 1999. Osmium isotope constraints on ore metal recycling in subduction zones. *Science* **286**, 512–516.

Manikyamba, C., Balaram, V., Naqvi, S.M., 1993. Geochemical signatures of polygenecity of banded iron formation of the Archaean Sandur greenstone belt (schist belt), Karnataka Nucleus, India. *Precambrian Res.* **61**, 137–164.

Manikyamba, C., Naqvi, S.M., 1996. Evidence of Archaean crustal shortening from deformed pillow lavas: an example from Sandur greenstone belt, Dharwar craton. *Curr. Sci.* **71**, 476–479.

Manikyamba, C., Naqvi, S.M., 1997. Late Archaean mantle fertility: constraints from metavolcanics of the Sandur schist belt, India. *Gondwana Research* **1**, 69–89.

Manikyamba, C., Naqvi, S.M., Moeen, S., Gnaneswar Rao, T., Balaram, V., Ramesh, S.L., Reddy, G.L.N., 1997a. Geochemical heterogeneities of metagreywackes from the Sandur schist belt: implications for active plate margin processes. *Precambrian Res.* **84**, 117–138.

Manikyamba, C., Naqvi, S.M., Sawkar, R.H., 1997b. Identification of Sandur schist belt as a potential gold field. *Current Science* **72**, 515–518.

Manikyamba, C., Kerrich, R., Naqvi, S.M., Ram Mohan, M., 2004. Geochemical systematics of tholeiitic basalts from the 2.7 Ga Ramagiri-Hungund composite greenstone belt, Dharwar craton. *Precambrian Res.* **134**, 21–39.

McLennan, S.M., Taylor, S.R., 1991. Sedimentary rocks and crustal evolution: tectonic setting and secular trends. *J. Geol.* **99**, 1–21.

Mukhopadhyay, D., Matin, A., 1993. The structural anatomy of the Sandur schist belt-a greenstone belt in the Dharwar craton of South India. *J. Struc. Geol.* **15**, 309–322.

Mukhopadhyay, D., Matin, A., 1996. Comment on the paper "The Sandur schist belt and its adjacent plutonic rocks — implications for late Archaean crustal evolution in Karnataka" by Brian Chadwick, V.N. Vasudev and Nazeer Admad, *J. Geol. Soc. India*, 47, 633–635.

Naqvi, S.M., 2005. *Geology and Evolution of the Indian Plate (From Hadean to Holocene – 4 Ga to 4 Ka)*. Capital Publishing Company, New Delhi, p.450.

Naqvi, S.M., Rogers, J.J.W., 1987. *Precambrian Geology of India*. Oxford University Press, New York, p. 223.

Naqvi, S.M., Condie, K.C., Allen, P., 1983. Geochemistry of some unusual early Archaean sediments from Dharwar craton, India. *Precambrian Res.* **22**, 125–147.

Naqvi, S.M., Sawkar, R.H., Subba Rao, D.V., Govil, P.K., Gnaneshwar Rao, T., 1988. Geology, geochemistry and tectonic setting of Archaean greywackes from Karnataka Nucleus, India. *Precambrian Res.* **39**, 193–216.

Naqvi, S.M., Manikyamba, C., Gnaneswar Rao, T., Subba Rao, D.V., Ram Mohan, M., Sarma, D.S., 2002a. Geochemical and Isotopic constraints of Neoarchaean fossil plume for evolution of volcanic rocks of Sandur greenstone belt, India. *J. Geol. Soc. India* **60**, 27–56.

Naqvi, S.M., Uday Raj, B., Subba Rao, D.V., Manikyamba, C., Nirmal Charan, S., Balaram, V., Sarma, D.S., 2002b. Geology and geochemistry of arenite-quartzwacke from the late Archaean Sandur schist belt-implications for provenance and accretion processes. *Precambrian Res.* **114**, 177–197.

Nesbitt, H.W., Young, G.M., 2004. Ancient climatic and tectonic settings inferred from paleosols developed on igneous rocks. In: Eriksson, P.G., Altermann, W., Nelson, D.R., Mueller, W.U., Catuneanu, O. (Eds.), *The Precambrian: Tempos and Events, Developments in Precambrian Geology 12*. Elsevier, Amsterdam, pp. 482–493.

Nutman, A.P., Chadwick, B., Krishna Rao, B., Vasudev, V.N., 1996. SHRIMP U/Pb Zircon ages of acid volcanic rocks in the Chitradurga and Sandur groups and granites adjacent to the Sandur schist belt, Karnataka. *J. Geol. Soc. India* **47**, 153–164.

Ohmoto, H., 2004. The Archaean atmosphere, hydrosphere and biosphere. In: Eriksson, P.G., Altermann, W., Nelson, D.R., Mueller, W.U., Catuneanu, O. (Eds.), *The Precambrian: Tempos and Events, Developments in Precambrian Geology 12*. Elsevier, Amsterdam, pp. 361–388.

Pears, J.A., Peate, D.W., 1995. Tectonic implications of the composition of volcanic arc magmas. *Annu. Rev. Earth Planet. Sci. Lett.* **23**, 251–285.

Peucat, J.J., Bouhallier, H., Fanning, C.M., Jayananda, M., 1995. Age of the Holenarsipur greenstone belt, relationship with the surrounding gneisses (Karnataka, South India). *J. Geol.* **103**, 701–710.

Plank, T., Langmuir, C.H., 1998. The chemical composition of subducting sediment and its consequences for the crust and mantle. *Chem. Geol.* **145**, 325–394.

Polat, A., Kerrich, R., Wyman, D.A., 1998. The late Archaean Schreiber-Hemlo and White River-Dayohessarah greenstone belts, Superior Province: college of oceanic plateaus, oceanic arcs and subduction-accretion complexes. *Tectonophysics* **294**, 295–326.

Polat, A., Kerrich, R., Wyman, D.A., 1999. Geochemical diversity in oceanic komatiites and basalts from the late Archaean Wawa greenstone belts, Superior Province, Canada: trace element and Nd isotope evidence for a heterogeneous mantle. *Precambrian Res.* **94**, 139–173.

Radhakrishna, B.P., Naqvi, S.M., 1986. Precambrian continental crust of India and its evolution. *J. Geol. Soc. India* **94**, 145–166.

Rudnick, R.L., Gao, S., 2004. Composition of the continental crust. *Treatise on Geochemistry* **3**, 1–64.

Simonson, B.M., Hassler, S.W., 1996. Was the deposition of large Precambrian iron formations linked to major marine transgressions? *J. Geol.* **104**, 665–676.

Subba Rao, D.V., Naqvi, S.M., Manikyamba, C., Balaram, V., Ram Mohan, M., 2001. Geological and geochemical characteristics of banded iron formation hosted gold mineralisation from Copper mountain belt, Sandur schist belt, Dharwar Craton. In: Subba Rao, K.V., Rajasekhar reddy, D. (Eds.), *Some Aspects of Mineral Developments of India*. Geol Soc India, pp. 67–82.

Sun, S.-S., McDonough, W.F., 1989. Chemical and isotopic systematics of oceanic basalts: implications for mantle composition and processes. In: Saunders, A.D., Norry, M.J. (Eds.), *Magmatism in the Ocean Basins*. Geol. Soc. Sp. Publ., pp. 313–345.

Taylor, S.R., McLennan, S.M., 1981. The composition and evolution of the continental crust: rare earth element evidence from sedimentary rocks. *Philos. Trans. R. Soc. London A.* **301**, 381–399.

Taylor, S.R., McLennan, S.M., 1985. *The Continental crust: Its Composition and Evolution*. Blackwell, Oxford, 307p.

Taylor, S.R., McLennan, S.M., 1995. The geochemical evolution of the continental crust. *Rev. Geophys.* **33**, 241–265.

Trendall, A.F., 1983. The Hamersley basin. In: Trendall, A.F., Morris, R.C. (Eds.), *Iron Formation: Facts and Problems*. Elsevier, Amsterdam, pp. 69–129.

Trendall, A.F., Blockley, J.G., 2004. Precambrian Iron-formation. In: Eriksson, P.G., Altermann, W., Nelson, D.R., Mueller, W.U., Catuneanu, O. (Eds.), *The Precambrian: Tempos and Events, Developments in Precambrian Geology 12*. Elsevier, Amsterdam, pp. 403–420.

Wronkiewicz, D.J., Condie, K.C., 1987. Geochemistry of Archaean shales from the Witwatersrand Supergroup, South Africa: Source-area weathering and provenance. *Geochim. Cosmochim. Acta* **51**, 2401–2416.

Wronkiewicz, D.J., Condie, K.C., 1989. Geochemistry and provenance of sediments from the Pongola Supergroup, South Africa: evidence for a 3.0 Ga old continental craton. *Geochim. Cosmochim. Acta* **53**, 1537–1549.

Wyman, D.A., Bleeker, W., Kerrich, R., 1999. A 2.7 Ga komatiite low- Ti tholeiite arc tholeiite transition and inferred proto-arc geodynamic setting of the Kidd Creek deposit: evience from precise ICP-Ms trace element data. *Econ. Geol. Monog.10*, 511–528.